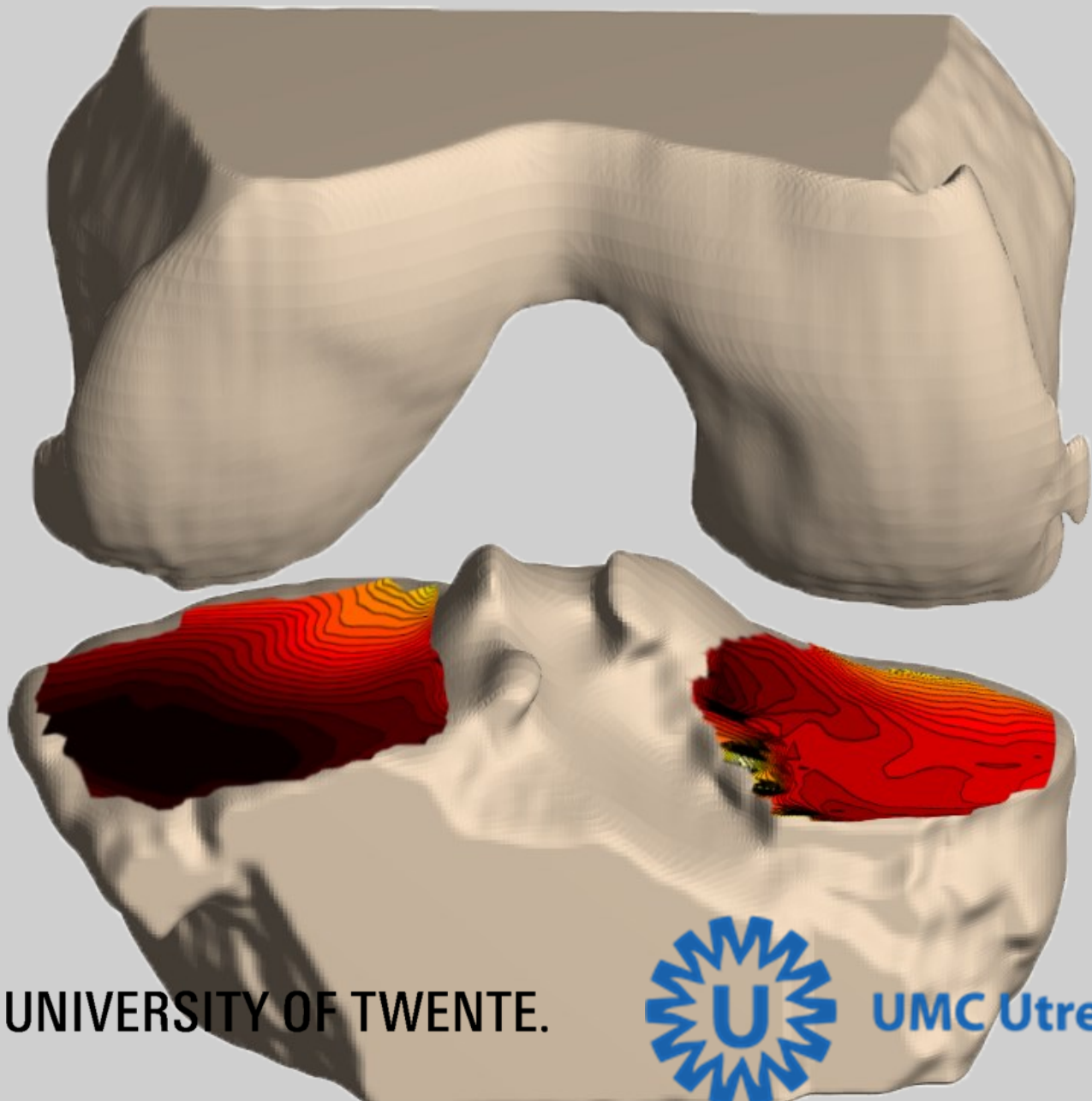


Technical Medicine Master of Science Thesis

A NOVEL 3D JOINT SPACE QUANTIFICATION METHOD IN PATIENTS WITH OSTEOARTHRITIS IN THE KNEE

Mylène Jansen, BSc



UNIVERSITY OF TWENTE.



UMC Utrecht

A novel 3D joint space quantification method in patients with osteoarthritis in the knee

Mylène Jansen, BSc
September 15, 2017

*Technical Medicine, Medical Imaging and Interventions
University of Twente
Enschede, The Netherlands*

*Department of Rheumatology
University Medical Center Utrecht
Utrecht, The Netherlands*

UNIVERSITY OF TWENTE.



Graduation Committee

Chairman	Prof.dr. H.B.J. Karperien <i>University of Twente, Enschede, The Netherlands</i>
Clinical Supervisor	Dr. W.E. van Spil <i>UMC Utrecht, Utrecht, The Netherlands</i>
Technical Supervisor UMC	Prof.dr. F.P.J.G. Lafeber <i>UMC Utrecht, Utrecht, The Netherlands</i>
Technical Supervisor UT	Prof.dr. H.B.J. Karperien <i>University of Twente, Enschede, The Netherlands</i>
Daily Supervisor	Dr. S.C. Mastbergen <i>UMC Utrecht, Utrecht, The Netherlands</i>
Daily Supervisor	N.J. Besselink, MSc <i>UMC Utrecht, Utrecht, The Netherlands</i>
Process Supervisor	Drs. P.A. van Katwijk <i>University of Twente, Enschede, The Netherlands</i>
External Member	Dr.ir. F.F.J. Simonis <i>University of Twente, Enschede, The Netherlands</i>

Preface

Six years of studying and seven years as a student are coming to an end with this thesis. Years in which I have learned not only theoretical matters, but have developed practical skills, gained experience doing research and found my way in clinical practice. I have been given the chance to develop myself not just during my studies, but also by being an active student, doing a board year at AEGEE-Enschede and living with fourteen other people in Huize NGTV'21. Not once during these years have I doubted my choice for studying Technical Medicine.

The past year I have been doing my graduation internship at the Rheumatology department at the UMC Utrecht. Having done an internship there before, I knew what to expect, and I knew I would love it. Now, one year later, I can present my Master's thesis, but it would not have been possible without the help of many others.

First of all, I would like to thank my supervising duo Nick & Simon. A technical physician himself, Nick Besselink always seemed to know exactly what to focus on and how to balance the medical and technical sides of my research. He was also a pro at subtly letting me know when I was being too optimistic or pessimistic at my results and gave me a great deal of helpful feedback on my thesis. Simon Mastbergen helped me a lot thinking about practical implications instead of just nice looking images and by steering me back to the core of my research, and always reserved some time for me when I needed help.

Erwin van Spil, thank you for being a great role model on making patients feel comfortable and for making me feel comfortable and self-assured when doing polyclinic. You always took time to answer my questions, even when time was short. I also want to thank Floris Lafeber for asking many critical questions and making me rethink topics that I thought I had completely figured out.

Thank you Paul van Katwijk, for being my mentor the past two years, making me talk about myself even when I did not want to and helping me realize my wish of doing an internship in Boston. Also a thank you to Elyse Walter, for being my mentor for half a year and Skyping with me while I was in the US.

Frank Simonis, thank you for helping me with my MRI study and being flexible during this 'happy chaos' as you called it, and for giving me feedback on the MRI part of my thesis. Marcel Karperien, I know we did not meet a lot, but in the few short times I saw you, I always left your office with helpful input and a new idea.

A huge thank you to all the amazing people of the Rheumatology department, for making me feel at home, making great coffee, helping me with many different things and for welcoming me to come and join you as a PhD candidate after my graduation.

Last but not least, the biggest thanks to my parents, my stepparents and my 'little' brother, for always helping me and listening to both my celebratory happiness when things went great and my complaining when they did not. I could not have done any of this without you and your many years of support. Sonia, thank you for making me take time off and relax, and for always, always making me laugh.

Mylène Jansen

Abstract

Introduction

In patients with knee osteoarthritis, cartilage loss causes a joint space width (JSW) decrease between the femur and tibia, which can be measured to quantify the disease progression or the effects of joint sparing treatments such as high tibial osteotomy (HTO) and knee joint distraction (KJD). This is currently done using radiographs, but possible alternatives to give insight in the JSW distribution throughout the joint are CT and MRI, 3D imaging techniques for which a measuring method must be developed and validated. Since CT and MRI images are taken non-weight-bearing with an extended leg, as opposed to weight-bearing, semi-flexed radiographs, the effects of weight-bearing and flexion on the knee joint space should be investigated.

Materials & Methods

Forty patients treated for knee OA (20 KJD, 20 HTO) were included. Radiographic outcomes and clinical characteristics were evaluated and CT and MRI scans were performed at baseline, one-year, and two-year follow-up. The JSW was measured on the radiographs and a 3D measurement method was developed to quantify the joint space in CT and MRI images. This semi-automatic method segments bone and generates heat maps and histograms to provide more insight in the joint space distribution. The JSW measurements were compared between imaging techniques and two-year changes were compared with clinical parameters.

In an additional MRI study, four different MRI scans were performed on healthy volunteers: a weight-bearing scan with extended and flexed leg and a non-weight-bearing scan with extended and flexed leg. Qualitative inspection of heat maps was performed to gain insight in JSW distribution changes.

Results

Correlations between radiographic and CT JSW were significant and strong while correlations of two-year JSW changes were not. Radiographic measurements agreed with two-year clinical parameter change better than CT measurements did.

The MRI study showed a shift of smaller joint space distances to the posterior side when flexing and more small distances when weight-bearing.

Discussion & Conclusion

The developed semi-automatic 3D JSW measurement method can quantify the 3D joint space from all available scans with minimal user input and visualize the joint space distribution throughout the joint. The weak longitudinal correlation of 3D JSW measurements with radiographs and clinical parameters cannot be directly explained from the available data, but the joint space changes observed in the MRI study with healthy volunteers indicate that differences in weight-bearing and knee flexion between the imaging methods could be the key to explaining the found differences. Therefore, additional MRI research with OA patients is necessary.

Contents

1	Introduction	1
1.1	Osteoarthritis	1
1.2	Treatment	2
1.3	Imaging methods	3
1.3.1	Radiography	4
1.3.2	Computed Tomography (CT)	4
1.3.3	Magnetic Resonance Imaging (MRI)	4
1.3.4	Ultrasound (US)	4
1.3.5	Comparing JSW quantification between imaging techniques	5
1.4	Quantifying the three-dimensional joint space	6
1.4.1	In-slice (2D) measurements in 3D images	6
1.4.2	3D measurements in 3D images	6
1.4.3	Current 3D JSW quantification method	7
1.5	Research objectives	8
2	Materials & Methods	11
2.1	Study population	11
2.1.1	Weight-bearing MRI study	12
2.2	Image acquisition	13
2.2.1	Weight-bearing MRI study	13
2.3	Clinical parameters	13
2.4	Measuring joint space width in radiographs	13
2.5	Development of a semi-automatic 3D measurement method	14
2.5.1	Bone segmentation and 3D reconstruction	14
2.5.2	Perpendicular and distance calculation	16
2.5.3	Output	18
2.6	Visual scoring	20
2.7	2D over-projection	20
2.8	Statistics	21
2.8.1	Demographics	21
2.8.2	Cross-sectional analysis	21
2.8.3	Longitudinal analysis	21
2.8.4	Minor confounders	21
2.9	Analysis of joint space variation between the weight-bearing and non-weight-bearing knee and the flexed and extended knee	22
2.10	Materials	22
3	Results	23
3.1	Demographics	23
3.2	Cross-sectional analysis	23
3.3	Longitudinal analysis	24
3.4	Minor confounders	26
3.5	Explorative MRI study: The effect of weight-bearing and knee flexion on the joint space	26
3.5.1	Flexion	26

CONTENTS

3.5.2	Weight-bearing	27
3.5.3	Radiograph position compared to CT position	28
4	Discussion & Conclusion	29
	References	33
	Appendix A Detailed Explanation of Methods	37
A.1	Bone Segmentation	37
A.2	Automatic Edge Fixing	43
A.3	Considerations	48
	Appendix B Technical details of performed scans	51
B.1	Radiographs	51
B.2	CT scans	51
B.3	MRI scans	51
	Appendix C MRI suitability form	53

Introduction

The knee is a complex and important joint in the human body. It must enable movement in the form of flexion and extension while simultaneously providing stability and handling the weight of the human body [1]. The knee consists of two parts: the femorotibial joint, between the femur (thighbone) and tibia (shinbone); and the patellofemoral joint, between the patella (kneecap) and femur. The femorotibial joint is the largest joint in the human body and the most important joint in the knee [2]. An overview of the joint is shown in figure 1.1. The medial and lateral condyles of the femur are positioned above the medial and lateral tibial condyles. The tubercles of the intercondylar eminence form the inner borders of the tibial condyles. The femur and tibia do not directly touch but are separated by the medial and lateral menisci (not imaged) and articular cartilage, which is present to create a smooth surface to decrease friction and enable the transmission of loads on the joint to the underlying subchondral bone [3]. Normal joint use and stress can cause gradual cartilage thinning [4], but this cartilage degeneration is worse than normal in patients with osteoarthritis.

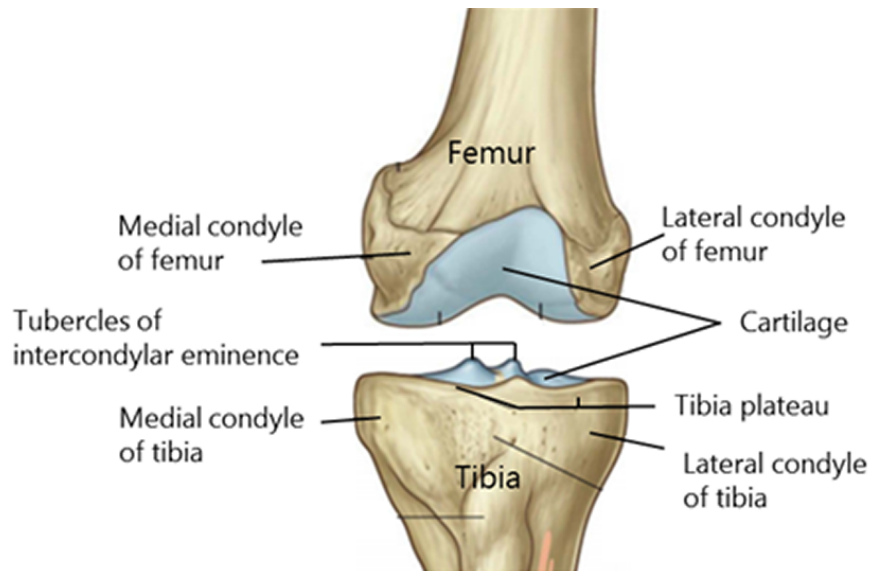


Figure 1.1: Overview of the tibiofemoral joint. Drawing taken from *Gray's Basic Anatomy* [5].

1.1 Osteoarthritis

Osteoarthritis (OA) is a joint disease that is highly prevalent in elderly: 15.6% of men and 30.5% of women over 55 years are affected by knee OA in The Netherlands, while osteoarthritic changes are present in most people over 70 [6, 7]. OA primarily effects weight-bearing joints such as the hip or knee and eventually causes joint pain and dysfunction. It is characterized by degeneration of articular

cartilage, remodeling and sclerosis of subchondral bone, and formation of osteophytes (bone spurs), but also affects the synovium, menisci and ligaments [8–11]. These changes are illustrated in figure 1.2. Risk factors for OA include obesity [12], female gender [13], aging [14], physical activity [15], positive family history [16] and prior knee injury [17], while varus and, to a lesser degree, valgus alignment of the knee can promote OA in either the medial or lateral compartment of the joint [18, 19]. Joint pain is the most common symptom why patients seek medical care, but the other symptoms can be present long before experiencing pain and seeking medical help [6, 20].

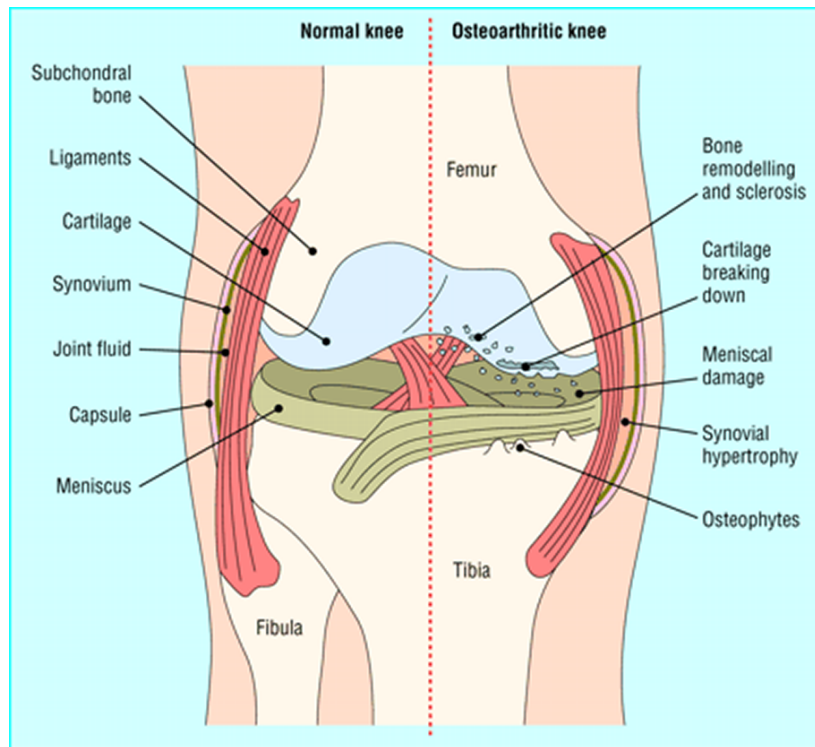


Figure 1.2: Changes in osteoarthritic joints [10].

Diagnosis of knee OA is mainly done based on clinical examination, symptoms and the previously mentioned risk factors [21], while the gold standard in imaging knee OA is currently weight-bearing radiography as recommended in European guidelines [22, 23]. These radiographs can show features like subchondral sclerosis and cysts that are characteristic for OA, but for the diagnosis and progression of the disease it is mostly the change in presence and size of osteophytes and the narrowing of the joint space width (JSW) that are being measured [24, 25]. The JSW is the distance between the tibia and femur and is useful for tracking the progression of the disease, since a decrease in JSW is an indirect measurement of cartilage degeneration in these patients. Furthermore, the change in JSW can be used to help determine the effectiveness of treatments for OA [26, 27]. The severity of OA can be described with the Kellgren-Lawrence scale [28] or the Osteoarthritis Research Society International (OARSI) classification score [29], both incorporating the previously mentioned characteristics of JSW decrease, osteophyte formation and bone sclerosis and remodeling.

1.2 Treatment

There is currently no treatment to cure OA or completely reverse the damage to cartilage and bone and most patients eventually undergo a total knee replacement (TKR) to manage the symptoms and improve quality of life [30, 31]. TKR is ideally postponed, however, since it has a limited durability, which is especially true for younger patients (<65) [32]. Replacement has a relatively high failure rate (18%), mainly because of infection [33]. Therefore, improvement of symptoms is first attempted with non-invasive means such as pain relief, physiotherapy and lifestyle changes [34]. TKR can be postponed with alternative surgical procedures aimed to improve the biomechanics of the joint. High tibial osteotomy (HTO) is a procedure for treating unicompartmental OA, where the disease is limited

to a single compartment in the knee often because of varus/valgus stance. This one side limitation is determined by pain experience and clinical examination as well as a radiographs displaying the leg axis and JSW measurements on both sides of the knee. By removing a wedge of bone from the tibia (closing wedge HTO) or adding an artificial wedge (opening wedge HTO, as seen in figure 1.3A), bone alignment in the knee is altered to relieve the most affected side, most often the medial side, and shifting weight towards the other side of the joint [35, 36]. Over time this should cause an increase of the JSW in the relieved side compared to natural OA progression.

A relatively new treatment option that can not only be used for unicompartmental OA but also when both sides of the joint are simultaneously affected by OA, as determined by clinical features and JSW measurements, is knee joint distraction (KJD). During KJD the femur and tibia are pulled apart five millimeters by an external fixation frame for six weeks, as seen in figure 1.3B, enabling cartilage regeneration both medially and laterally [37]. Compared to natural OA progression, this should cause an increase of JSW on both sides of the joint. Clinical studies show a minimal JSW increase of 59% (0.57mm, 95%CI 0.09 – 1.06; $p=0.03$) over two years compared to baseline [38] and even five years after treatment, the increase in minimal JSW after KJD was statistically significant compared to the estimated natural OA progression (difference in change after five years +0.59mm, 95%CI:+0.17-+1.02; $p=0.009$) [39].

For both KJD and HTO, the JSW does not necessarily increase after treatment. This is especially true for HTO, since it is not directly based on cartilage regeneration. However, since both treatments cause an increase in JSW compared to natural OA progression, the change in JSW can be used to track the progression of OA as well as the effectiveness of the chosen treatments. Different imaging methods are available to analyze the JSW change.

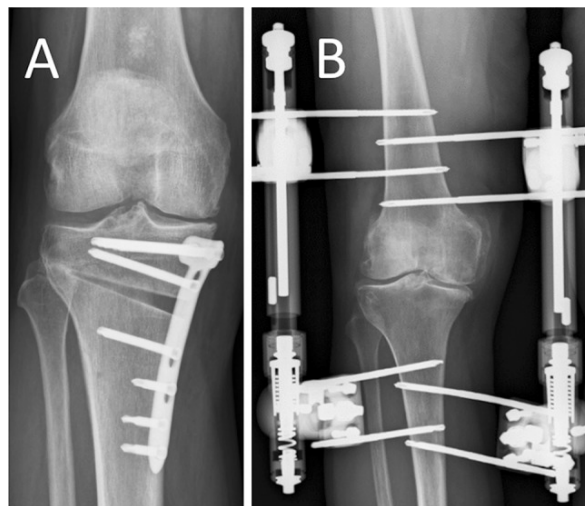


Figure 1.3: Example of different treatments of knee OA, with radiographs of (A) a patient treated with HTO and (B) a patient treated with KJD [40].

1.3 Imaging methods

Since OA is a disease that primarily effects cartilage, imaging the cartilage directly would be preferable. However, cartilage is non-calcified tissue and is surrounded by other types of soft, non-calcified tissue, such as menisci, tendons and ligaments [41]. This makes distinctively imaging and automatically detecting cartilage in the images difficult. In contrast, bone is hard, calcified tissue and therefore more easily imaged and distinguished from other tissues [42]. Considering that cartilage cannot be imaged as easily as bone, the cartilage degeneration (or regeneration) can be quantified by measuring the distance between the bony ends of the joint and expressed as changes in joint space width. There are different imaging modalities available to image the joint space and quantify the JSW, and they are described in the next subsection.

1.3.1 Radiography

Currently anteroposterior or posteroanterior radiographs, made while the patient is standing (weight-bearing), are the gold standard to image the osteoarthritic knee. JSW measurements in these radiographs can be performed in different ways, but all of them are two-dimensional measurements in the frontal view of the knee. Distances are measured between the lower border of the femur and the tibia plateau. However, displaying a three-dimensional knee in a two-dimensional image causes over-projection, where different parts of the knee are imaged on top of each other. This makes it difficult to determine where on the tibia plateau the distances to the femur should be measured. Often either the frontal ridge of the tibia [43] or the floor of the tibia plateau [44] is used. Other important considerations for radiographs are the angle of the knee while the image is taken (flexion angle) [45] and the angle at which the x-ray beam is aimed at the knee (beam inclination) [46]. Variations in these variables will affect the JSW measurement results: 10 degrees of knee flexion results in a 12.5% increase in JSW measurements compared to an extended knee, while a 10-degree difference in x-ray beam can cause a 20.4% difference in measured JSW [46]. These variations are of great influence in case longitudinal images are needed, where especially the positioning of the patient is of importance. As stated before, osteophytes and changes in subchondral bone can also be analyzed on radiographs [24, 25]. A typical example of a radiograph of an osteoarthritis patient can be seen in figure 1.4A.

1.3.2 Computed Tomography (CT)

Like radiography, Computed Tomography (CT) uses radiation to image bone clearly. Contrarily to radiography, CT is a three-dimensional imaging technique, able to image the entire knee in multiple two-dimensional slices. Another important difference with radiography is that a CT scan is almost always performed with the patient is lying down (non-weight bearing), since normal CT scanners are not able to scan patients that are standing. Scans are made with a straight (extended) leg. An example of one slice of a CT scan of an osteoarthritis patient can be seen in figure 1.4B.

1.3.3 Magnetic Resonance Imaging (MRI)

Magnetic Resonance Imaging (MRI), like CT, is a three-dimensional imaging technique that mostly scans patients lying down with a straight leg (non-weight-bearing extended). Making MRI scans of patients that are standing is possible, but requires a special MRI scanner that is not often available in standard clinical practice. Unlike radiography and CT, MRI can image soft tissue as well, including cartilage and menisci, although this still needs optimization especially in defining the exact borders of these structures [47]. An example of one slice of an MRI scan of an osteoarthritis patient can be seen in figure 1.4C.

1.3.4 Ultrasound (US)

Ultrasound (US) is a cheap and fast imaging method that has been described to successfully detect changes in the amount of fluid present in the joint [48], inflammation (synovitis) [49] and even osteophytes [50]. However, it is not a good imaging method to measure cartilage changes or joint space width changes, mostly because of the lack of protocol on how to measure it [48], resulting in a high variability between the assessed pathology and definitions and grading for pathology [49]. Furthermore, the images are taken with a relatively small US beam that is used from multiple angles and has no bone penetration, limited soft tissue penetration and cannot show the uneven cartilage distribution on the entire tibia plateau, since the knee is a relatively big joint [51]. For these reasons, ultrasound is not further considered in this thesis.



Figure 1.4: A radiograph (A), CT slice (B) and MRI (Eckstein) slice (C) of the left knee of one patient.

1.3.5 Comparing JSW quantification between imaging techniques

Radiography, the gold standard, has the advantages of fast scanning, low costs and the fact that the scans are made weight-bearing (standing), which could cause a significant difference in measurement results compared to a non-weight-bearing (lying down) image as is made with CT and MRI. Weight-bearing scans could be a more realistic representation of what the patient is experiencing while walking or standing. Measurements could be influenced by knee flexion as well: radiographs are taken with a slightly flexed knee while CT and MRI are performed with a straight (extended) leg. Kan et al [52] found that the mean JSW was significantly smaller for flexed knees compared to extended knees, with a mean of 3.02 mm for flexed knees and 4.31 mm for fully extended knees. According to clinicians, a typical radiography exam takes around 5 minutes, while CT and MRI scans take around 15 minutes. JSW measurement time is around 10 minutes for radiography [53] and 5 minutes for CT and MRI, since these techniques allow for (partly) automatic measurements and therefore require less manual input. CT and MRI, being three-dimensional imaging techniques, allow for distance measurements throughout the entire knee joint, unlike in radiography where the three-dimensional knee is over-projected into a two-dimensional image. Limited literature is available on comparing inter- and intra-observer variability between radiography, CT and MRI. Marchant et al [54] report kappa values for bone identification on all three imaging techniques. A kappa value of 1 indicates perfect agreement between measurements, while a value of 0 means there is no agreement other than expected by chance. As shown in table 1.1, kappa values showed CT to have an excellent inter- and intra-observer variability, while values were the lowest for radiography. In radiography, there can be variation X-ray beam inclination as well as the knee flexion angle while taking the radiograph, which both will change the imaged joint space, although standardized protocols can decrease this [45, 46, 55, 56]. The decision where to measure the JSW in the radiograph is also subject to variability since it is not done automatically, although protocol adherence and radiography experience can again partly compensate for this [46, 53]. MRI can image soft tissue like cartilage and menisci, although precise defining of their borders remains difficult [47], while CT excels at imaging bone density. Lastly, there is no radiation involved in MRI while radiation is low for both radiography and CT, due to development of ultra-low dose CT [57]. Table 1.1 summarizes the most relevant advantages and disadvantages when using radiography, CT and MRI for quantification of JSW in patients with knee OA.

Table 1.1: Comparison of using radiography, CT and MRI for OA patients. Bold cells indicate the best performing imaging method for different properties.

	Radiography	CT	MRI
Scan time	Low (~5 min)	Medium (~15 min)	Medium (~15 min)
Cost	Low	Low/Medium	High
Weight-bearing	Yes	No (possible, but not accessible)	No (possible, but not accessible)
Measurement time	Medium (~10 min)	Low (~5 min)	Low (~5 min)
Inter- and intra-observer variability	Kappa: intra- 0.53, inter- 0.16	Kappa: intra- 1.00, inter- 1.00	Kappa: intra- 0.61, inter- 0.17
Three-dimensional	No	Yes	Yes
Image soft tissue	No	No	Yes
Image bone density	No	Yes	No
Radiation	Low	Low/Medium	None

3D imaging is not often used for quantifying JSW, therefore lacking clear definitions on what exactly the joint space width is, what the (relevant) boundaries of the joint space are and in what way the distances should be measured.

1.4 Quantifying the three-dimensional joint space

Two-dimensional joint space quantification has been extensively studied and protocolled, making it relatively straightforward measuring the tibiofemoral joint space on radiographs. For the purpose of proper three-dimensional joint space quantification, a literature study has been performed. Search terms used include *CT*, *MRI*, *knee*, *JSW*, *joint space width*, *3D*, *measurement*, *tibia*, *femur*, *OA*, *osteoarthritis* and *tibiofemoral*. Articles were included when describing the use of a 3D imaging technique to measure JSW in the knee or a similar joint translatable to the knee. Both in-slice (2D) measurements and 3D measurements were included and the different methods are described below.

1.4.1 In-slice (2D) measurements in 3D images

Agnesi et al [58] measure the smallest medial and lateral distance between the tibia and femur in every slice, which means the measurement is two-dimensional. The minimum distances from all slices were combined to calculate the average, median, minimum and maximum distance for both sides of the joint. Foumani et al [59] implement a different method, measuring the perpendicular distances between two bones in the wrist (radiocarpal) joint as illustrated in figure 1.5A. They measure at multiple locations in every slice, but since it is done separately for every slice, the measurements are still two-dimensional. All measured distances throughout the joint are averaged to a mean JSW.

1.4.2 3D measurements in 3D images

Several three-dimensional measurement methods have been used in literature, though no general review of the possibilities has been written. In all these methods, the bone is first selected (segmented) and saved on every slice. Subsequently, a three-dimensional reconstruction of the bones is made. These reconstructions are then used for the distance measurements.

Tamez-Peña et al [60] calculate the distances perpendicularly between the femur condyles and the tibia surface. This means it is similar to the method Foumani et al [59] used (figure 1.5A) but the measurements are performed in 3D. A distance map is created and the medial and lateral distances are averaged. Van IJsseldijk et al [61] create a new coordinate system based on the orientation of the tibia plateau, making the tibia plateau the horizontal bottom of the coordinate system (i.e. the tibia plateau is positioned in the xy-plane at $z = 0$). The distances are calculated perpendicularly from the tibia plateau (along the z-axis) to the femur, illustrated in figure 1.5B. Since all distances are calculated in a single direction it is not a fully three-dimensional method, while the use of the 3D bone reconstruction makes it more three-dimensional than the in-slice measurements are. Lastly, a method that is used often is calculating the shortest three-dimensional distance to the femur from many points on the tibia surface [62–64]. This method is illustrated in figure 1.5C. From these measurements, a

distance map can be created and numbers such as the average medial and lateral distance and the percentage of distances that is smaller than a certain threshold value.

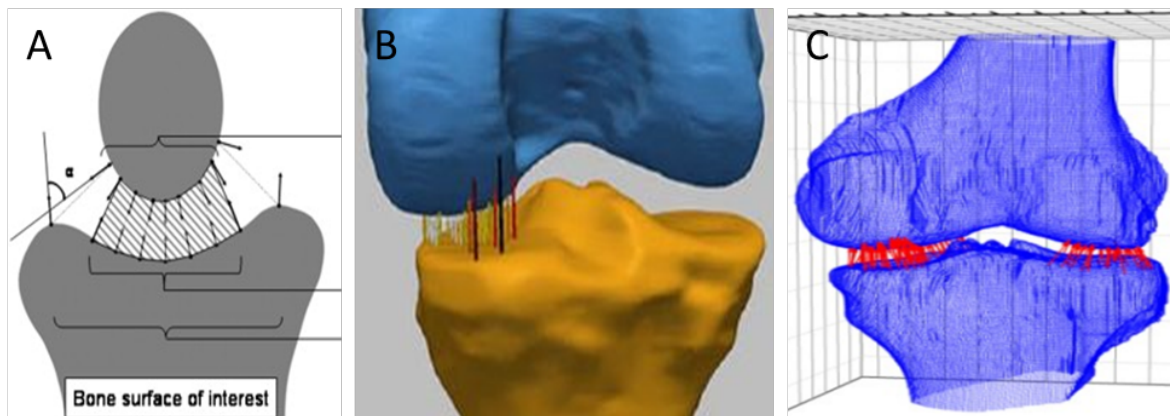


Figure 1.5: Three different joint space width measurement methods. In (A) the perpendicular distances between two bones are used to two-dimensionally calculate the JSW [59]. In (B) the vertical distances from reconstructed, three-dimensional tibia to femur are used to calculate the JSW [61]. In (C), the shortest distances from the reconstructed tibia to femur are used to three-dimensionally calculate the JSW [62].

1.4.3 Current 3D JSW quantification method

For the current study a fully three-dimensional measurement method was preferable, meaning a 3D reconstruction of the bones is made and the measurements are not solely done in a predetermined plane. It uses the available 3D data more optimally by allowing measurements in all directions instead of being limited to only the axial direction. Perpendicular distance measurements were chosen for two main reasons.

Firstly, this method takes the bone shapes into account. When standing or walking, body weight presses the femur onto the tibia. The force transfer in the joint is an important factor in knee osteoarthritis [65] and will depend on the bone shapes as well as connected soft tissue like tendons, menisci and cartilage. The forces cause a temporary and eventually permanent degenerative trigger to the cartilage. Over time, these compressions will alter the surface and alignment of the bone. Therefore, it makes sense to take the bone shapes into account when measuring the joint space width. The shape of the tibia seems the most important since it is the receiving surface, and studies that focus on tibiofemoral forces measure the forces from the perspective of the tibia plateau as well [66–68]. This means the distances should be measured perpendicularly from the tibia surface.

The second reason is that perpendicular measurements automatically define the boundaries of the joint space. It is difficult to determine where the measured distances are relevant and where they are not, since some parts in the joint are important for keeping the knee in the correct position or enabling certain movements, but are not necessarily weight-bearing. This in turn makes the definition of joint space difficult. None of the articles from the literature study explain how the borders of the joint space were chosen. Defining joint space distances as the perpendicular distance from the tibia surface to the femur means that only parts of the tibia surface where there is a perpendicular distance to measure are included as joint space, see figure 6. In this example perpendiculars from the tibia are drawn in a single sagittal slice of the knee in two dimensions. Perpendiculars are displayed from multiple parts of the tibia, but the distance for each perpendicular can only be calculated if it reaches the femur. If it does, this perpendicular and thus the part of the tibia where it is calculated from, the origin, is included in the joint space (green arrows). If it does not and the femur is not in the perpendicular line trajectory, no distance can be calculated and the part of the tibia where this perpendicular originates from is not included in the joint space (red arrows).



Figure 1.6: Two-dimensional perpendiculars from the tibia surface to the femur are defining what is included in the joint space (green arrows, because they hit the femur) and what is not (red arrows, because they miss the femur).

While figure 1.6 shows a two-dimensional slice and perpendiculars, it works the same for a three-dimensional reconstructed tibia and femur and three-dimensional perpendiculars. Fully automatically determining the external boundaries of the joint space is a big advantage since it prevents inter- and intra-user variation. This fact, combined with the previously highlighted reason that perpendicular measurements take the shape of the tibia into account, is why the perpendicular method was chosen to define three-dimensional joint space and the distances belonging to this joint space.

Summarizing, osteoarthritis is a disease that is mainly characterized by cartilage degeneration. Current cartilage imaging is inaccurate, therefore the change in distance between the tibia and femur is used as a substitute measure for cartilage degeneration in different imaging techniques. The gold standard for measuring JSW is a weight-bearing, semi-flexed radiograph, but possible alternatives that have not been investigated extensively thus far are CT or MRI, three-dimensional imaging methods. These methods are usually made in non-weight-bearing and fully extended conditions, however, which could influence measurement results. In order to quantify the 3D joint space with minimal inter- and intra-user variability, the distances to the femur perpendicular from the tibia surface can be measured. This method is preferred because it takes the bone shape into account, which could be important in dividing the pressure between the bones and thus for the cartilage degeneration as a result of this pressure.

1.5 Research objectives

The primary objective for this research was defined as follows:

Develop and validate a (semi-)automatic method for measuring the joint space width in three dimensions in patients with osteoarthritis in the knee.

The 3D measurement method could be developed either automatic or semi-automatic, requiring some user input. The outcome and results of this three-dimensional method must then be validated by comparing with the results as measured using radiographs, since this is the current gold standard. Additionally, both methods can be compared with clinical results. The influence of confounders on these comparisons should be investigated as well. Possible minor confounders consist of available demographic data such as BMI, age, leg axis (varus/valgus) or the initial severity of OA (Kellgren & Lawrence score) for every patient and these are relatively easy to correct for. Major confounders are weight-bearing and knee flexion angle, since these factors could cause significant JSW measurement differences between the semi-flexed weight-bearing radiographs and extended non-weight-bearing CT

and MRI scans. Since the influence of these factors has not yet been investigated, follow-up research is warranted.

Following these considerations, additional secondary objectives were defined:

- Develop a (semi-)automatic method for measuring the joint space width in three-dimensional images
- Compare measurement results with radiographs (the gold standard) and medical findings and determine the influence of major and minor confounders
- Qualify the effect of weight-bearing and flexion on the joint space in the knee in a proof-of-principle study in a healthy population

Materials & Methods

The approach used to answer the primary and secondary research questions are described in this chapter. For the development of the (semi-)automatic 3D method and the comparison with radiographs, the main study population, image acquisition and clinical parameters were used as described below. To gain insight into the joint space changes between the weight-bearing and non-weight-bearing knee and the flexed and extended knee, a separate MRI study was performed. Therefore, a different study population and image acquisition are described for this part.

2.1 Study population

Patients were included originating from two independent randomized controlled trials (RCT) [40, 69]. Patients with medial compartmental knee OA considered for HTO according to regular practice, randomized to either KJD or HTO (1:2), were asked to participate in this extended imaging study. Due to the relatively low number of KJD versus HTO patients, caused by the 1:2 randomization ratio, KJD patients from an RCT comparing TKP with KJD were additionally supplemented to this study. These patients were, according to regular practice, considered for TKP surgery and randomized to either KJD or TKP (1:2). This rendered a total of 40 KJD and 40 HTO patients, of whom half consented to an extended imaging study and were included in the current study population. An overview of the combined studies is shown in figure 2.1.

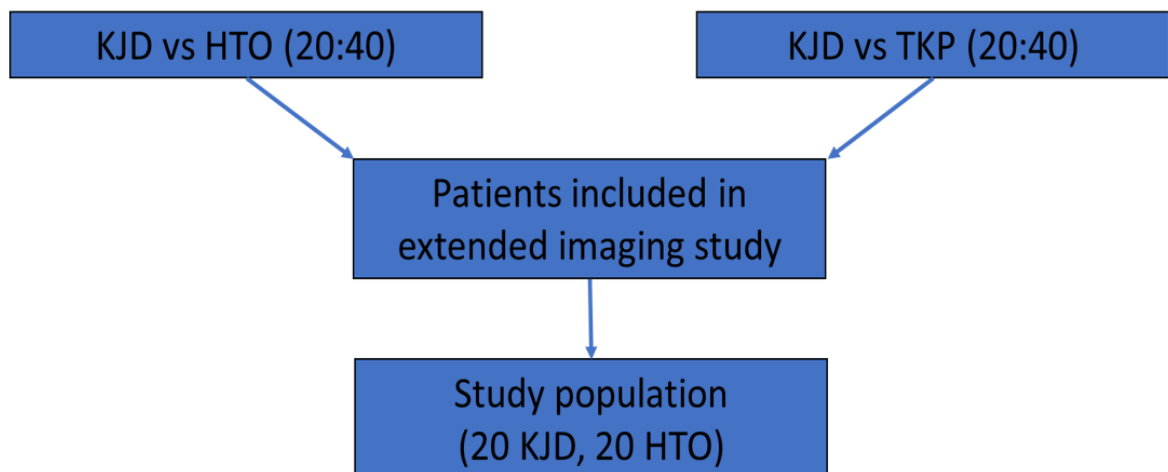


Figure 2.1: Overview of the studies combined to form the study population of 20 KJD patients and 20 HTO patients.

The in- and exclusion criteria used for the studies are listed below [70, 71]. Most criteria were identical for the two different studies. Criteria specific for the KJD versus HTO study are indicated with (HTO) while criteria specific for the KJD versus TKP study are indicated with (TKP):

Inclusion criteria:

1. (HTO) Patients with medial or lateral tibio-femoral compartmental OA considered for HTO according to regular clinical practice
2. (TKP) Patients considered for TKP according to regular clinical practice
3. Age <65 years
4. Radiological joint damage: Kellgren & Lawrence score above 2
5. Intact knee ligaments
6. (HTO) Normal range-of-motion (min. of 120° flexion)
7. (TKP) Normal range-of-motion (min. of 120° flexion; max flexion limitation of 15°)
8. Normal stability
9. Body Mass Index <35

Exclusion criteria:

1. (HTO) Mechanic axis-deviation (varus-valgus) of less than 10 degrees
2. Psychological inabilities or difficult to instruct
3. Not able to undergo MRI examination (standard daily clinical practice protocol)
4. Inflammatory or rheumatoid arthritis present or in history
5. Post traumatic fibrosis due to fracture of the tibial plateau
6. Bone-to-bone contact in the joint (absence of any joint space on X-ray)
7. Surgical treatment of the involved knee <6 months ago
8. (HTO) Contra-lateral knee OA that needs treatment
9. (TKP) An infectious susceptible prosthesis (joint replacement) in situ
10. Primary patello-femoral OA

Before treatment (baseline), the age, BMI and leg axis (varus/valgus) of every patient was recorded. Evaluations consisted of image acquisition, clinical and radiographic outcome measures, acquired at baseline, 12 months, and 24 months after treatment. Patients undergoing HTO did not undergo a CT and MRI scan at 12 months due to the plate in situ.

2.1.1 Weight-bearing MRI study

In the proof-of-principle MRI study, healthy volunteers were included with the following in- and exclusion criteria:

Inclusion criteria:

1. Age between 18 and 40 years
2. Suitable to be scanned in an MRI scanner according to the MRI form in appendix C
3. Able to give informed consent
4. Able to stand without assistance for ten minutes

Exclusion criteria:

1. Condition in the knee that is expected to cause JSW changes
2. Metal present near the knee that can cause artifacts

For these volunteers, their BMI and global varus/valgus stance are registered. Four different scans are made, as described in section 2.2.1.

2.2 Image acquisition

The image acquisition for the HTO/KJD study population as described in section 2.1 consisted of radiographs, CT scans and MRI scans according to protocols explained in more detail below. Appendix B contains more technical details of the different scans.

Radiographs

Standardized semi-flexed weight-bearing radiographs acquired at baseline were used to determine the Kellgren & Lawrence grade according to guidelines [28] and radiographs acquired at baseline, one year and two years to evaluate changes in JSW over time. The knee is positioned in such a way that the tibia plateau is seen as horizontal (in front view), according to the protocol of Buckland-Wright [72]. A dedicated software package, Knee Images Digital Analysis (KIDA) [53], was used to evaluate JSW over time by a single experienced observer, providing four JSW measures; mean JSW of the total joint (mean JSW), mean JSW of the medial and lateral compartment (respectively medial JSW and lateral JSW), and minimal JSW of the whole joint (minimal JSW).

CT

Standardized, non-weight-bearing CT scans of the extended knee were acquired at baseline and two years after treatment, with an additional scan one year after treatment for patients treated with KJD. The scans were made on three different scanners, with a slice thickness of either 1 or 2 mm and a pixel size varying from 0.29x0.29 mm to 0.79x0.79 mm.

MRI

Standardized, non-weight-bearing MRI scans of the extended knee were acquired at baseline and two years after treatment, with an additional scan one year after treatment for patients treated with KJD. The scans were made using a Philips Achieva 3T scanner with the 3D Eckstein protocol, resulting in a slice thickness of 1.5 mm and a pixel size of 0.31x0.31 mm.

2.2.1 Weight-bearing MRI study

For the additional MRI study to analyze the difference between weight-bearing and non-weight-bearing, the rotatable Esaote G-scan Bio 0.25T with a 4-channel knee coil was used. Scans were made with the 3D SHARC protocol [73], creating images with a slice thickness of 0.59 mm and a pixel size of 0.59x0.59 mm and thus enabling cubic voxels. A small field of view (FOV) of 150x150 mm was chosen to ensure a high resolution while keeping scan time low (3:20 min).

2.3 Clinical parameters

Clinical effectiveness was determined by the Western Ontario & McMaster Universities Osteoarthritis Index (WOMAC 3.0) derived from the Knee Injury and Osteoarthritis Outcome Score (KOOS) questionnaire (self-assessment reduced from five to three dimensions and using a five-point Likert scale, normalizing to a 100-point scale, where 100 is optimal). The WOMAC is divided in scales for pain (WOMAC pain), stiffness (WOMAC stiff), function (WOMAC function) and a total scale combining these three (WOMAC total). Additionally, pain is measured by implementing the Visual Analogue Scale for Pain (VAS Pain), a continuous scale ranging from 0 (no pain) to 100 (worst imaginable pain), upon which the patient indicated the amount of pain. Both the WOMAC and VAS questionnaire were performed at baseline, one year and two years after treatment for all patients.

2.4 Measuring joint space width in radiographs

Joint space width in radiographs was measured using Knee Images Digital Analysis (KIDA) software [53]. To measure the JSW, the user manually positions four circles on the lower edge of the femur and four circles on the frontal ridge of the tibia and does this for both the medial and lateral side of the joint (figure 2.2). The program automatically calculates the distances between each vertical pair of circles and combines these to determine the previously mentioned measures (mean JSW, minimal JSW, medial JSW and lateral JSW).

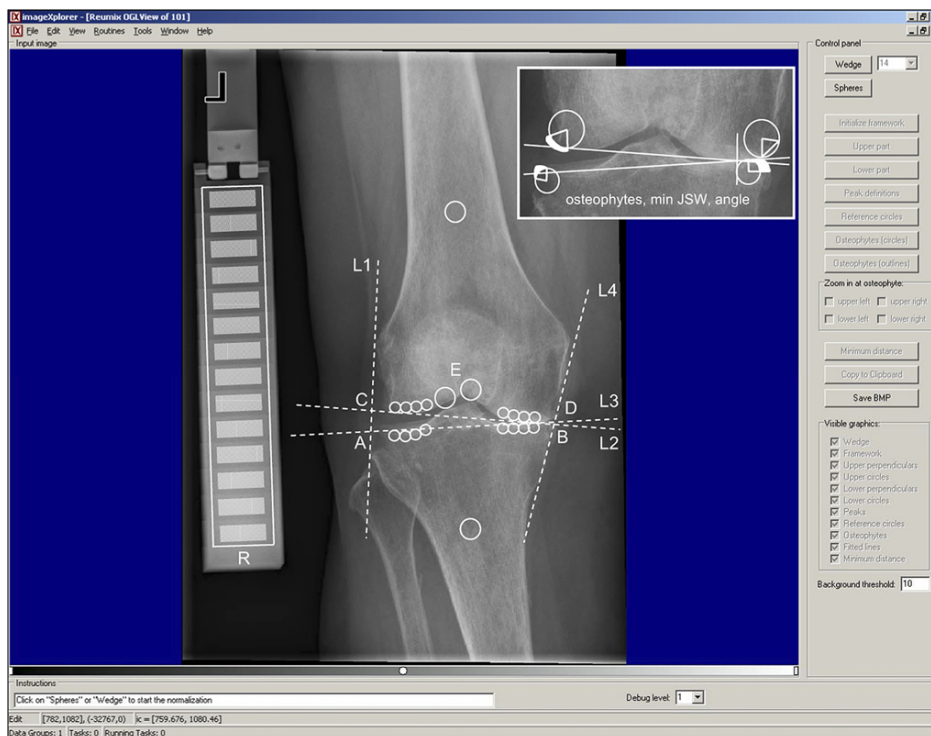


Figure 2.2: Presentation of KIDA by Marijnissen et al [53]. The 16 small circles are placed manually to calculate the JSW.

2.5 Development of a semi-automatic 3D measurement method

Developing the measurement method consists of three parts: segmenting the bone from the separate slices and making a three-dimensional reconstruction, calculating the perpendiculars from the tibia surface and corresponding distances to the femur and producing visual output and JSW measurement numbers. The entire method was developed to work on all 3D imaging methods. Below, the three parts of the method are explained globally. A more elaborate and technical explanation can be found in appendix A of this thesis.

2.5.1 Bone segmentation and 3D reconstruction

To create a three-dimensional reconstruction of the femur and tibia, the bone must be selected from the different image slices. Only the part of the images where the joint space is located is used by letting the user draw a rectangular region of interest in the central slice, as shown in figure 2.3A.

To segment bone, Canny edge detection [74] is used. This method detects edges in images by finding abrupt changes in intensity between pixels, as is the case for the transition between bone and surrounding soft tissue. The automatic detection is done slice by slice and in every slice the user checks and, if necessary, corrects the marked edges as they are displayed on the corresponding slice (figure 2.3B). After the user confirms the edges are detected correctly, the bone is segmented (figure 2.3C) and the program moves on to the next slice, incorporating the bone segmentation from the previous slice to improve automatic detection, until the user indicates the end of the joint has been reached.

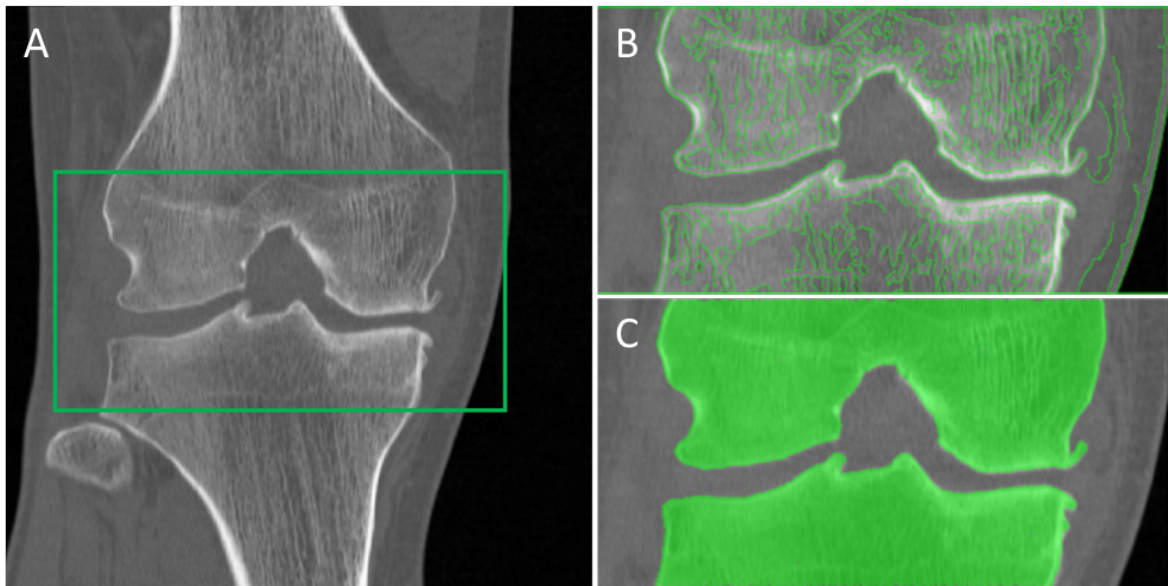


Figure 2.3: Bone segmentation in the first (middle) slice. (A) Original slice with rectangle where the user defines the joint space, (B) edges originally detected on the image and (C) the final segmented bone in this slice.

The bone segmentation is the only part that requires user input by checking the automatically detected edges, the rest of the semi-automatic method is performed fully automatically. To ensure the reconstructed bone shape represents the bone shape realistically, the segmented 3D data is smoothed. This means the transition between slices will be more gradual and small changes in bone will be less abrupt.

After segmentation and smoothing of the data, the 3D reconstruction of the bones is made. As can be seen in figure 2.4, the objects are constructed of many small triangles (faces). Interaction points between these faces are called vertices.

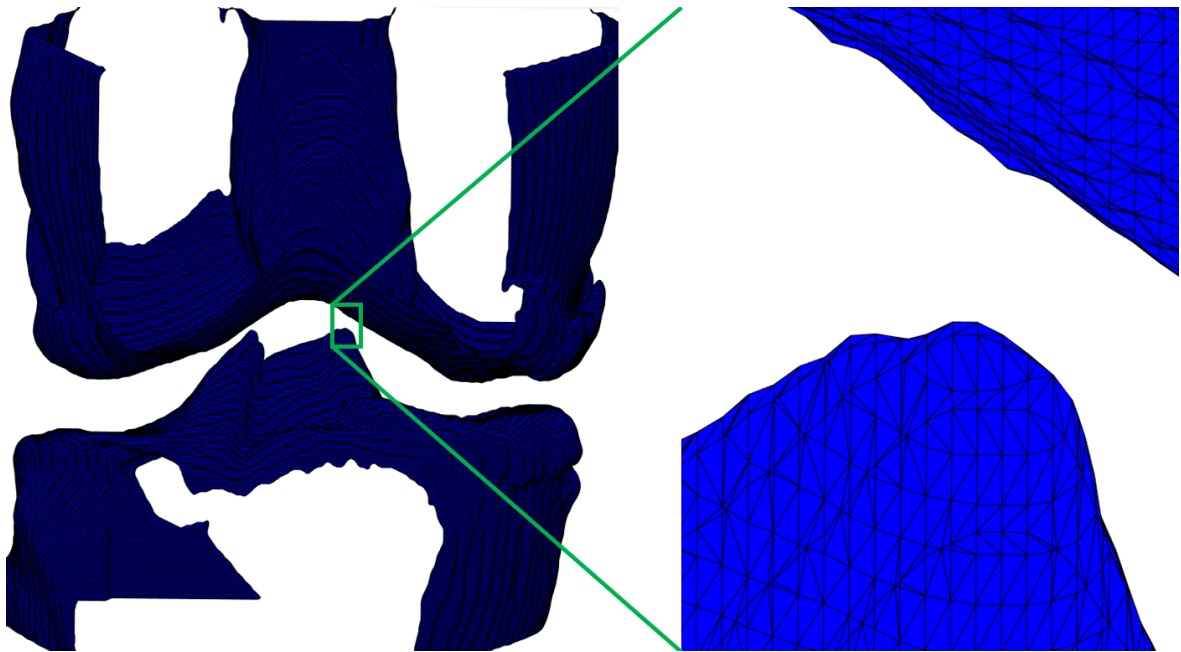


Figure 2.4: 3D Reconstruction of tibia and femur, with a close-up to show the structure of vertices and faces.

2.5.2 Perpendicular and distance calculation

After the 3D reconstruction, the perpendiculars are automatically calculated from the tibia surface. These perpendiculars are calculated first for all faces that make up the surface, after which these vectors are used to create new vectors coming from all vertices. The perpendiculars originating at the tibia plateau's vertices and pointing upwards in axial direction are used for the next steps. To make sure that small irregularities on the tibia surface will not cause the perpendiculars to point in a direction that does not realistically present the force transfer, the perpendiculars are averaged over a predetermined number of square millimeters. For optimal distribution throughout the tibia plateau, corresponding with the local surface but ignoring small irregularities, each perpendicular represents a tibia surface area of 2x2 mm (figure 2.5A). Perpendicular calculation and averaging is done similarly for the reconstructed femur.

Parts of the tibia surface that are not subjected to force transfer between the tibia and femur should not be included in the representative the joint space. The tibia perpendiculars that should be excluded are not consistent between scans, because it is dependent of the exact anatomy and the knee position in which the scan was taken. Therefore, only perpendiculars with the femur in the line's trajectory are included. Additionally, for every perpendicular from the tibia surface that reaches the femur, it is checked at what location it reaches the femur's surface. The femur perpendicular originating from this location, should also have the tibia in its trajectory. If not, the original point at the tibia plateau is excluded from the joint space, since there is no mutual force transfer between the tibia and femur at that location. This methodology mostly excludes large distances at the posterior side of the joint, where tibia perpendiculars reach the back of the femur instead of the bottom of the femur condyles. Possibly perpendiculars should only be included if the angle between the tibia perpendicular and the femur perpendicular originated near the point where the tibia perpendicular reaches the femur is small enough. Though it has not been done for the perpendiculars used in this study, it is possible to limit this angle if desired, to possibly more precisely specify where direct force transfer between the tibia and femur occurs. Examples of inclusion choices are shown in figure 2.6. The place on the tibia plateau where the red perpendicular in this figure originated would be excluded in this research, while both the yellow and green perpendiculars would be included. Defining a limit of a certain angle between α and β would exclude the yellow pair but include the green pair. The perpendiculars of interest coming from the tibia plateau are color coded according to the corresponding distance from the origin on the tibia plateau to the femur, as seen in figure 2.5B.

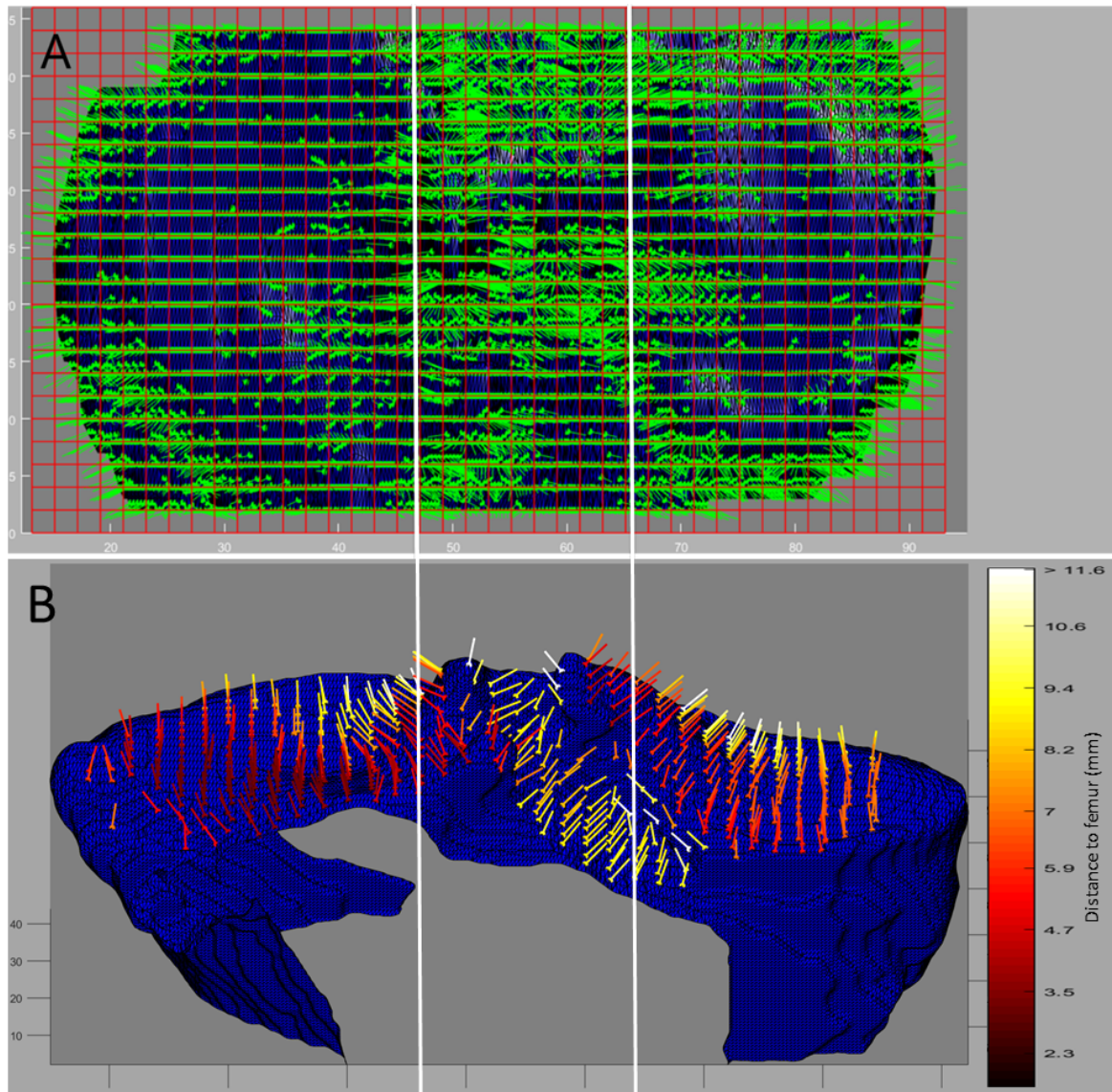


Figure 2.5: (A) All perpendiculars and their origins (green) pointing upwards from the tibia plateau (blue) that are averaged over areas of 2x2 mm as indicated with the grid (red). (B) The averaged perpendiculars with the femur in the line's trajectory, of which the matching femur perpendicular has the tibia in its trajectory, color coded according to the distance from their origin on the tibia plateau to the femur, as indicated by the color bar. The white lines display the cut-off when dividing the plateau and perpendiculars in lateral and medial, as described in the end of section 2.5.3.

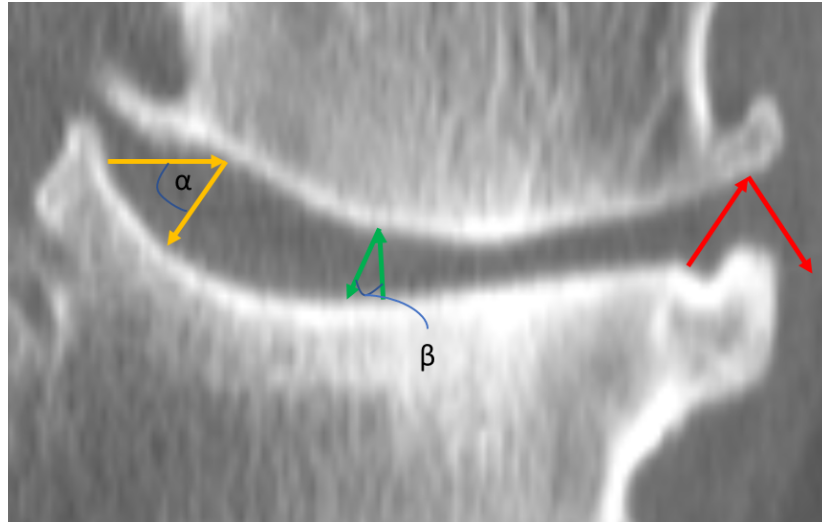


Figure 2.6: Different perpendicular inclusion options. The red arrows show a pair of perpendiculars where the tibia perpendicular reaches the femur at a certain place, but the femur perpendicular originating from this place does not reach the tibia. The green and yellow arrows show perpendicular pairs where the femur perpendicular does reach the tibia, with different angles (β and α , respectively) between the two perpendiculars.

2.5.3 Output

There are many ways to display or calculate the joint space distances. One visualization method is to smoothen the distances to the femur at the origin positions throughout the joint in a heat map, shown as a top view of the tibia plateau as seen in figure 2.7 below. The heat map of one KJD patient at baseline, one year and two years after treatment are displayed, with the color bar indicating the interpretation of different colors. The change in joint space distances can then be judged visually.

Alternatively, to quantify the distances more objectively and determine global changes in JSW distribution, all distances in the joint space can be plotted in a histogram and the distribution of distances can be fitted to plot a line. Figure 2.8 shows an example of this method for the same patient as displayed in figure 2.7. As can be seen, the lower distances are on the left while the higher distances are on the right. A better result is indicated when the general plot and especially the peak in the line is positioned more to the right. When the differences are small and difficult to judge in the heat maps, the more objective histograms and line fits can display the differences in JSW distribution, though the location of distances in the joint is not incorporated.

Over the entire joint space as displayed in figure 2.7, several output numbers are generated. One can use any of these numbers, such as the mean and median of the distances and the minimum distance present, for statistics.

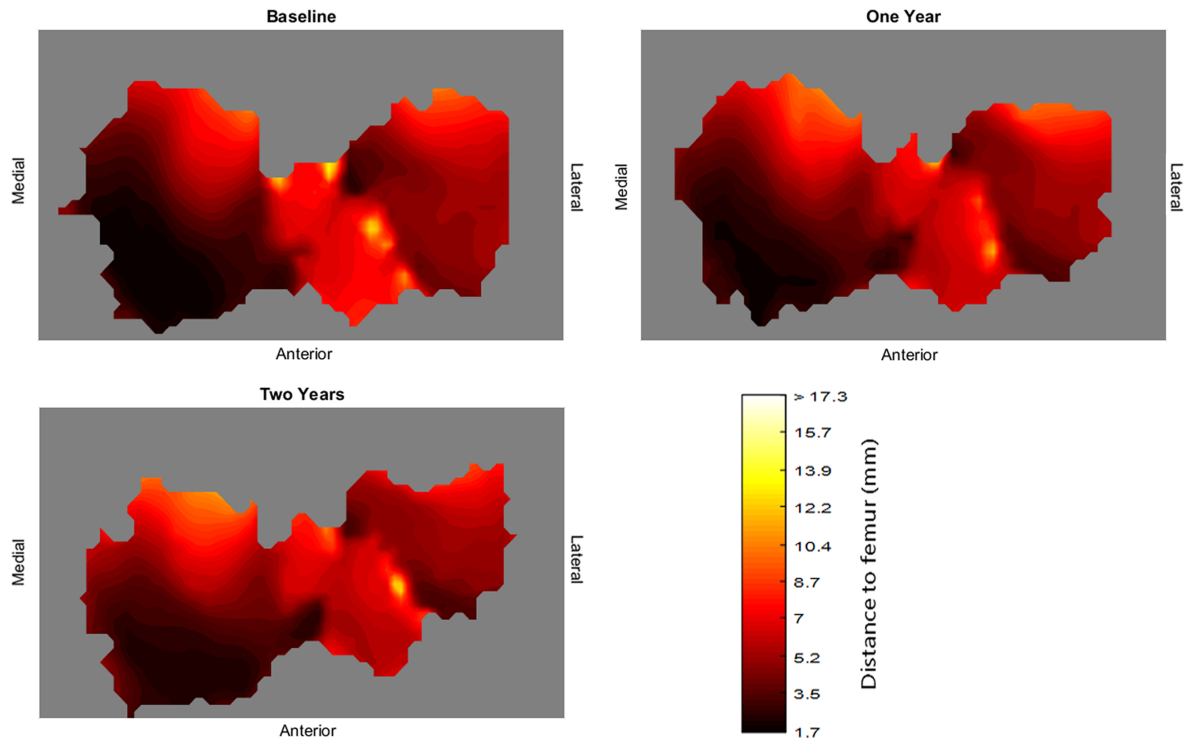


Figure 2.7: Heat maps of one patient treated with a KJD from CT images at baseline, one year and two years after treatment. The color bar indicates the significance of the different colors in millimeter distance from the tibia plateau to the femur.

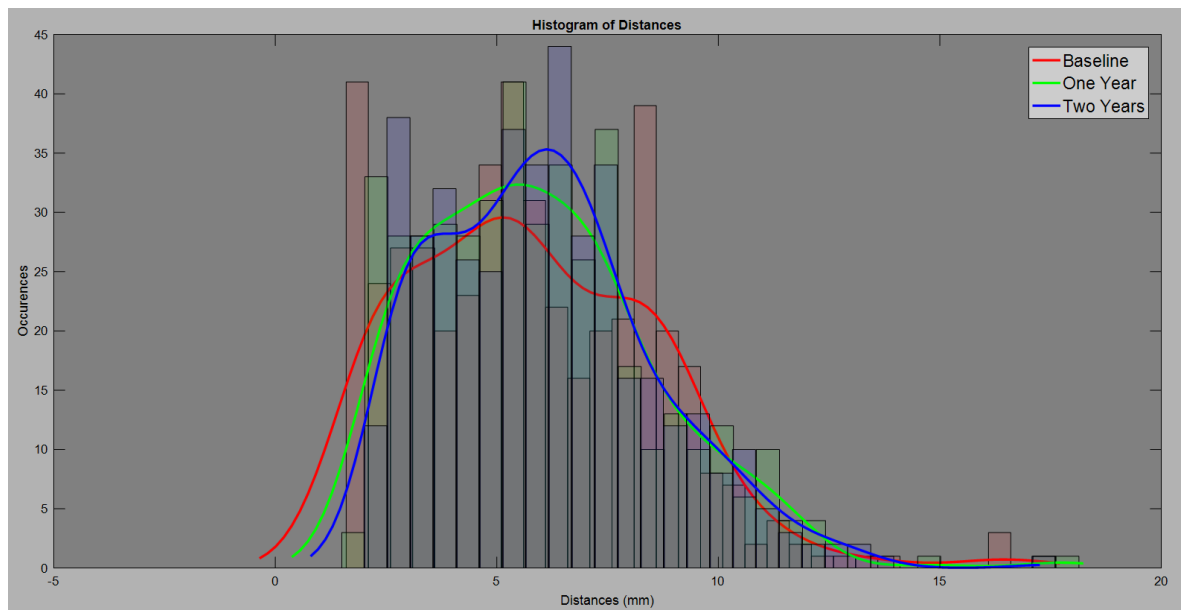


Figure 2.8: Histograms and fitted lines of same patient as shown in figure 2.7. The red bars and line represent the joint space distances throughout the entire joint at baseline, while green represents measurements one year after treatment and blue two years after treatment.

Instead of including the entire joint space in the output and considering it as a whole, it is also possible to split the measurements in the lateral and medial side. This is especially useful when comparing measurement results with KIDA measurements, since KIDA mainly uses medial and lateral results, and for analyzing the shift from one side to the other after HTO. Splitting the results is done by manually choosing where to place two straight, anteroposterior lines as middle borders and for this research, the place where the tubercles of the intercondylar eminence are at half of their maximum

height are chosen, since it was theorized that distances between the tubercles are less relevant (figure 2.5B). After splitting the data in medial and lateral, the mean and median of the distances and the minimum distance present on either side can be calculated.

2.6 Visual scoring

One way to compare the longitudinal change in joint space width for the 3D method with the longitudinal change for KIDA is by visually scoring the heat maps and comparing the general direction of the change (improvement or deterioration) with the direction for KIDA. Since visual scoring is subjective and expectations of changes over time for different treatments can cause a bias, the heat maps were randomized to show pairs of heat maps containing two time points of the same patients. Both the order of patients and the order of the time points were randomized. The resulting image pairs were independently scored by three different observers, by judging if the right image was much better, better, the same, worse or much worse compared to the left image. These scores were combined into one resulting score for every pair, which was then used to express the scores for the different time points for all patients.

2.7 2D over-projection

Since radiographs are taken weight-bearing and with a slightly flexed knee, while CT and MRI scans are performed non-weight-bearing with an extended leg, there could be differences when comparing imaging methods that are not related to the measurement method. Therefore, 2D over-projection images were simulated from the 3D bone reconstructions by rotating the reconstruction so that the tibia plateau was horizontal. An example can be seen in figure 2.9.

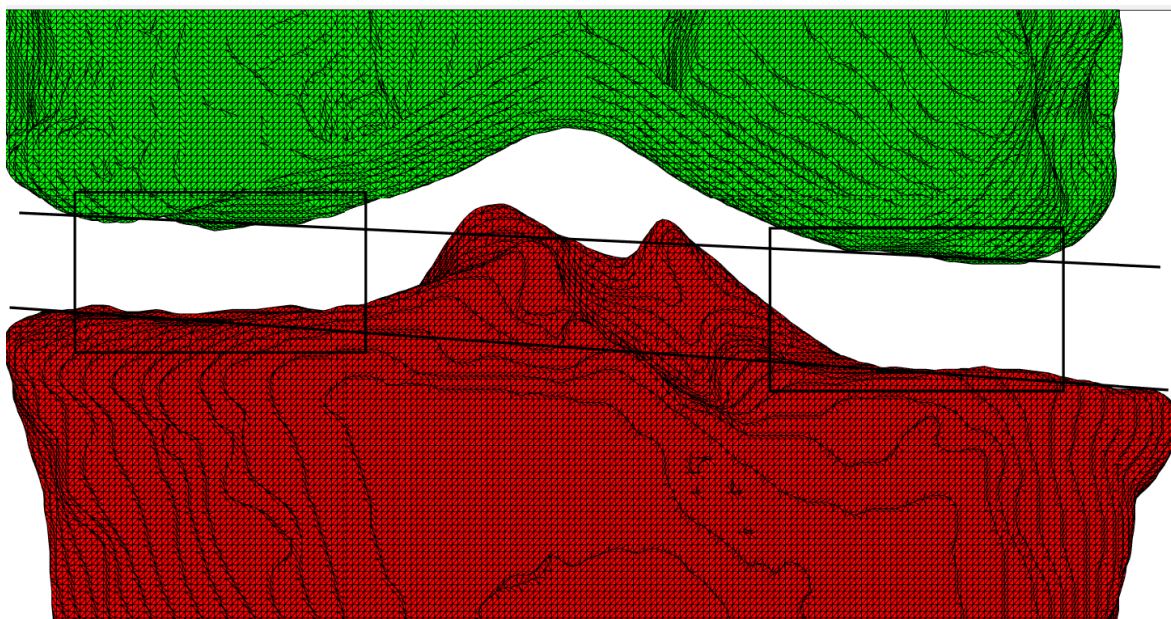


Figure 2.9: 2D over-projection view of the femur (green) and tibia (red), rotated so the tibia plateau is straight. The distances are measured between the top and bottom line, inside the left and right rectangle, to measure the joint space width similarly to KIDA for the medial and lateral side.

From this view, the distances between the tibia and femur for the medial and lateral side of the joint were calculated at the same positions as is done in KIDA [53]. The distances were calculated vertically between the top and bottom line in figure 2.9, inside the rectangles as seen in the figure to separate the medial and lateral side. The mean distance inside each rectangle was saved as the mean medial and lateral distance. Theoretically, differences found between these results and the KIDA results should derive solely from the difference in weight-bearing and knee angle.

2.8 Statistics

2.8.1 Demographics

The two different treatments, KJD and HTO, can cause different JSW longitudinal changes for the patients treated with either of these treatments. However, it must be ensured that there are no significant differences between the two treatment groups at baseline, before treatment, since this could have consequences unrelated to the treatment option. A paired samples t-test between the KJD and HTO group was performed for the parameters age, gender, BMI, leg axis, Kellgren & Lawrence score, maximum flexion, maximum extension, WOMAC scores, VAS score and mean medial, mean lateral, mean joint and minimum KIDA JSW.

2.8.2 Cross-sectional analysis

For all time points pooled together, KIDA JSW measurements were compared with 3D and 2D over-projection measurements from CT images. The Pearson correlation coefficient was calculated between the parameters as shown in table 2.1. For 3D CT, the median was chosen since the data was not normally distributed. KIDA mean, 3D CT median and 2D over-projection CT mean are referred to in the rest of this thesis simply as KIDA, 3D CT and 2D CT. All correlations were calculated for all patients together as well as separately for KJD and HTO patients. The mean and 95% confidence interval (95%CI) were calculated for all parameters and patient groups.

Table 2.1: Short overview of 3D CT and 2D over-projection CT parameters with which the lateral and medial mean KIDA were compared, using the Pearson correlation.

	3D CT	2D CT
KIDA lateral mean	Lateral median	Lateral mean
KIDA medial mean	Medial median	Medial mean

2.8.3 Longitudinal analysis

To compare the changes over time between KIDA and CT, the Pearson correlation was calculated, on group level, between the change in KIDA and the change in 3D CT values as well as the change in KIDA and the change in 2D CT values. The same parameters as mentioned in table 2 were used, but now as the change over time of these parameters (delta scores). The mean and 95% confidence interval (95%CI) were calculated for all parameters and patient groups. Furthermore, paired samples t-tests of these same values over time in KIDA and 3D CT were performed and compared. Additionally, the changes over time in the heat maps created from the 3D measurements, visually scored as described in section 2.6, were compared to the delta scores for mean KIDA distance over the entire joint. This was done for every patient and only the direction of the change (improvement/deterioration) was compared, not the amount of change. Since the heat maps are compared to the gold standard, the percentage of agreement can be scored with true positives and negatives, false positives and false negatives. Furthermore, both the change in the heat maps of the 3D CT outcome and KIDA joint delta scores were compared to the change in WOMAC and VAS score, to compare both techniques with the change in clinical parameters.

2.8.4 Minor confounders

Possible minor confounders considered in this study population are the patients' age, gender, BMI, leg axis (varus/valgus), the initial severity of OA (Kellgren & Lawrence score), maximum knee extension and flexion, total WOMAC score and total VAS score. Using linear regression, the influence of these possible confounders on the relation between the KIDA JSW and the 3D JSW is tested for the medial and lateral side, for KIDA taking the mean values of all these parameters and for the 3D JSW taking the median values. The same is done for the change over time of all these variables. All calculations were done on all patients together as well as separated in KJD and HTO patients.

2.9 Analysis of joint space variation between the weight-bearing and non-weight-bearing knee and the flexed and extended knee

Four different MRI scans were made of healthy volunteers in the study population for this experiment, to analyze the difference in joint space distribution in the knee between weight-bearing and non-weight-bearing and, additionally, between an extended and partly flexed leg. The volunteer is positioned in the scanner, with their left knee in the knee coil. The scanner is then rotated to a standing position (81 degrees) and the volunteer is scanned with their knee first as extended as possible and in a next scan slightly flexed to the maximum angle permitted (MAP) in the knee coil (>20 degrees). For both scans, the exact flexion angle was measured. After both standing scans, the MRI table is rotated back to the lying position (0 degrees). Again, a scan with a straight leg and a slightly flexed leg is made in the same way as was done for the standing position. A schematic overview of the scans is shown in figure 2.10.

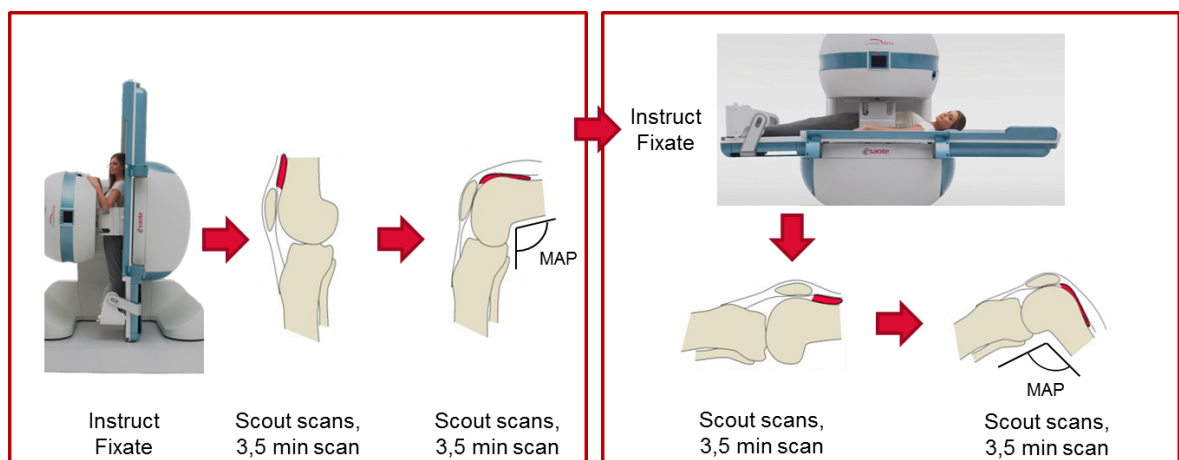


Figure 2.10: Overview of the different positions and scans for the MRI experiment. Volunteers are first scanned in standing position with the knee as extended as possible and flexed to the maximum angle permitted (MAP). The scanner is then rotated, to scan the volunteers lying down with the knee as extended as possible and flexed to the MAP.

Since the semi-automatic 3D measurement method was created to work on all 3D imaging methods, it can be applied directly to the MRI images obtained from the scanner. From the data, the same output can be produced as described in section 2.5.3.

This experiment is of an explorative nature: analysis of the scan results starts with a visual inspection of the heat maps and looking for pattern changes between scanning positions. The aim is not to look for statistically significant differences, but to gain insight into generalized changes in JSW distribution. Since clear pattern differences are expected, heat maps of different scanning positions are registered so an overlaying contrast image can be created. Direction vectors for the entire joint as well as both sides separately, calculated using singular value decomposition (SVD), are used to express the pattern change objectively. Only difference map values within the range of median \pm SD were used for the SVD, since this included most of the values while preventing large values to skew the direction excessively.

2.10 Materials

The commercial software package MATLAB (2016b, The MathWorks Inc., Natick, MA, 2000) was used for the development of the 3D measurement method, analysis of CT and MRI images and calculations on these images. The commercial software package SPSS (IBM Corp. Released 2012. IBM SPSS Statistics for Windows, Version 21.0. Armonk, NY: IBM Corp.) was used for all statistical calculations.

Results

3.1 Demographics

Of the original 40 patients consented to this imaging study, seven patients were lost to follow up for various reasons (e.g. no more participation or discovered comorbidity), leaving a total of 33 patients included in this research, of whom 16 patients were treated with KJD and 17 patients were treated with HTO. The demographic characteristics of the study participants are summarized in table 3.1.

Table 3.1: Demographic characteristics of study participants.

	KJD (n=16)	HTO (n=17)	Independent sample t-test
Age	53.3 (± 7.0)	49.2 (± 6.4)	p = 0.01
Gender (male/female)	66.7%/33.3%	(70.6%/29.4%)	p = 0.89
BMI	27.0 (± 3.6)	26.7 (± 2.8)	p = 0.81
Leg axis (varus in degrees)	4.1 (± 6.4)	6.9 (± 2.7)	p = 0.17
Kellgren-Lawrence	3.1 (± 0.8)	2.4 (± 0.8)	p = 0.02
Flexion	128.2 (± 10.1)	132.1 (± 9.4)	p = 0.27
Extension	2.3 (± 3.4)	2.6 (± 2.5)	p = 0.81
WOMAC stiffness	38.3 (± 15.3)	41.2 (± 20.6)	p = 0.65
WOMAC pain	46.2 (± 17.1)	46.5 (± 20.1)	p = 0.97
WOMAC function	48.2 (± 16.0)	49.7 (± 15.4)	p = 0.78
WOMAC total	50.0 (± 15.7)	48.3 (± 15.2)	p = 0.78
VAS	6.3 (± 1.70)	6.5 (± 1.7)	p = 0.83
KIDA medial	2.2 (± 2.8)	1.9 (± 1.2)	p = 0.71
KIDA lateral	7.7 (± 2.3)	7.6 (± 1.5)	p = 0.86
KIDA joint	4.9 (± 0.8)	4.7 (± 0.9)	p = 0.51
KIDA minimum	0.2 (± 0.5)	0.7 (± 1.1)	p = 0.15

3.2 Cross-sectional analysis

Medial JSW was smaller than lateral JSW for all treatments and measurement methods as seen in table 3.2. For both patient groups, KIDA medial JSW measurements were smaller than both CT medial JSW measurements while 2D CT medial JSW values were smaller than 3D CT medial JSW values. KIDA lateral JSW measurements were bigger than CT lateral JSW measurements and 2D CT lateral JSW values were smaller than 3D CT lateral JSW values.

Table 3.2: The mean and upper and lower boundary of the 95% confidence interval for the KIDA, 3D CT and 2D CT medial and lateral JSW values, calculated in millimeters for the two treatment groups KJD and HTO separately as well as all patients together.

	KJD		HTO	
	Medial (mm)	Lateral (mm)	Medial (mm)	Lateral (mm)
KIDA	2.9 (2.1;3.6)	7.9 (7.2;8.6)	2.4 (2.0;2.8)	7.5 (7.1;8.0)
3D CT	5.0 (4.6;5.4)	6.8 (6.4;7.1)	4.6 (4.3;4.9)	6.6 (6.3;6.9)
2D CT	3.8 (3.4;4.2)	5.5 (5.0;6.0)	3.5 (3.3;3.8)	5.9 (5.5;6.2)

As seen in table 3.3, KIDA measurements for medial JSW were strongly positively correlated to 2D CT and 3D CT JSW in the KJD group (both; $p < 0.001$). A moderate positive correlation was found when comparing KIDA lateral JSW with 2D CT and 3D CT JSW (both; $p < 0.01$). The same trend is seen in the HTO group. There was a moderate positive correlation between KIDA and 3D CT JSW for the medial and lateral side (both; $p < 0.01$). KIDA medial JSW was weakly positively correlated to 2D CT ($p = 0.04$) while KIDA and 2D CT measurements were not significantly correlated for the lateral side ($p = 0.20$).

For all patients grouped together, KIDA medial and lateral JSW were correlated moderately to strongly positively to both 3D CT and 2D CT (all; $p < 0.01$).

Table 3.3: Pearson correlation coefficients for the relationship between KIDA medial and lateral values and the 3D and 2D CT medial and lateral JSW values. The coefficients were calculated for all patients together as well as the two treatment groups, KJD and HTO. Bold values are significant ($p < 0.05$).

	Side	KJD		HTO		All	
		3D CT	2D CT	3D CT	2D CT	3D CT	2D CT
KIDA	Medial	R = 0.81 p < 0.001	R = 0.64 p < 0.001	R = 0.50 p < 0.01	R = 0.35 p = 0.04	R = 0.75 p < 0.001	R = 0.54 p < 0.001
	Lateral	R = 0.55 p < 0.001	R = 0.53 p < 0.01	R = 0.53 p < 0.01	R = 0.23 p = 0.20	R = 0.54 p < 0.001	R = 0.41 p < 0.01

3.3 Longitudinal analysis

As seen in table 3.4, the mean medial JSW increases over two years for KJD patients when measuring with KIDA (+0.9 mm) but a decreases when measuring with 2D CT (-0.3 mm), while no change was observed using 3D CT data (0.0 mm). The lateral JSW increases over two years for KJD patients for all measurement methods (KIDA +0.3mm; 3D CT +0.5 mm; 2D CT +0.1 mm). When looking specifically at the HTO treated patients, differences between imaging modalities were found. Using KIDA, the medial JSW increases over two years for HTO patients (+1.0 mm), but using 3D or 2D CT it decreases (both; -0.5 mm). The lateral JSW decreases using KIDA (-0.1 mm) or 2D CT (-0.2 mm), but increases using 3D CT (+0.1 mm).

Table 3.4: The mean and upper and lower boundary of the 95% confidence interval for the two-year delta values for KIDA, 3D CT and 2D CT medial and lateral values, calculated in millimeters for the two treatment groups KJD and HTO separately as well as all patients together.

	KJD		HTO	
	Δ Medial (mm)	Δ Lateral J(mm)	Δ Medial (mm)	Δ Lateral (mm)
KIDA	0.9 (0.4;1.6)	0.3 (-0.5;1.0)	1.0 (0.5;1.5)	-0.1 (-0.7;0.6)
3D CT	0.0 (-0.5;0.5)	0.5 (0.3;0.8)	-0.5 (-0.8;-0.2)	0.1 (-0.1;0.3)
2D CT	-0.3 (-0.7;0.2)	0.1 (-0.4;0.5)	-0.5 (-0.9;-0.1)	-0.2 (-0.6;0.3)

The moderate to strong correlation between KIDA and 3D CT and 2D CT mostly disappears when looking at two-year delta values. As can be seen in table 3.5, for KJD patients only the strong positive correlation between lateral KIDA and 3D CT JSW ($p < 0.01$) and the moderate positive correlation between medial KIDA and 2D CT JSW ($p < 0.05$) are significant. For HTO patients none of the correlations are significant and for all patients grouped together only KIDA lateral JSW is moderately positively correlated with 3D CT ($p < 0.01$).

Table 3.5: Pearson correlation coefficients for the relationship between the two-year delta scores of the KIDA medial and lateral values and the 3D and 2D CT medial and lateral values. The coefficients were calculated for all patients together as well as the two treatment groups, KJD and HTO. Bold values are significant ($p < 0.05$).

	Side	KJD		HTO		All	
		Δ 3D CT	Δ 2D CT	Δ 3D CT	Δ 2D CT	Δ 3D CT	Δ 2D CT
Δ KIDA	Medial	R = 0.30 p = 0.26	R = 0.50 p < 0.05	R = -0.15 p = 0.58	R = -0.10 p = 0.72	R = 0.13 p = 0.48	R = 0.23 p = 0.21
	Lateral	R = 0.67 p < 0.01	R = -0.21 p = 0.45	R = 0.22 p = 0.40	R = -0.28 p = 0.28	R = -0.28 p < 0.01	R = 0.48 p = 0.22

KJD led to a statistically significant increase in medial JSW for KIDA for both KJD (+0.97 mm, $p < 0.01$) and HTO (+1.02 mm, $p < 0.001$) patients, as seen in table 3.6. Using 3D CT, the KJD patients show a small, non-significant increase (+0.01 mm, $p = 0.98$) on the medial side, but HTO patients show a statistically significant medial decrease (-0.45 mm, $p = 0.01$). Thus, for HTO patients, KIDA and 3D CT measurements resulted in an opposite change over time for the medial side. For the lateral side, 3D CT shows a statistically significant increase in KJD patients (+0.54 mm, $p < 0.001$), while KIDA shows a non-significant increase (+0.27 mm, $p = 0.45$). For HTO patients neither technique shows a significant lateral change. Grouping all patients together shows a statistically significant medial increase in KIDA (+0.99 mm, $p < 0.001$) and lateral increase in 3D CT (+0.31 mm, $p < 0.001$). The changes in medial 3D CT (-0.23 mm, $p = 0.10$) and lateral KIDA (+0.09 mm, $p = 0.69$) were not significant.

Table 3.6: Results of paired samples t-tests between the medial and lateral KIDA (mean) and 3D CT (median) values two years after treatment and the same values at baseline before treatment. The tests were performed for all patients together as well as the two treatment groups, KJD and HTO, separately. Significant paired differences ($p < 0.05$) are bold.

		Paired differences			Sig. (2-tailed)
		Mean (mm)	95% Confidence Interval of the Difference		
			Lower (mm)	Upper (mm)	
KJD	Medial KIDA	0.97	0.39	1.56	p < 0.01
	Medial 3DCT	0.01	-0.49	0.50	$p = 0.98$
	Lateral KIDA	0.27	-0.47	1.02	$p = 0.45$
	Lateral 3DCT	0.54	0.30	0.79	p < 0.001
HTO	Medial KIDA	1.02	0.54	1.49	p < 0.001
	Medial 3DCT	-0.45	-0.75	-0.16	p = 0.01
	Lateral KIDA	-0.07	-0.74	0.59	$p = 0.82$
	Lateral 3DCT	0.09	-0.07	0.26	$p = 0.25$
All	Medial KIDA	0.99	0.64	1.35	p < 0.001
	Medial 3DCT	-0.23	-0.51	0.05	$p = 0.10$
	Lateral KIDA	0.09	-0.38	0.57	$p = 0.69$
	Lateral 3DCT	0.31	0.15	0.47	p < 0.001

As seen in table 3.7, the agreement of the visually scored heat map change direction with KIDA for KJD patients is high for changes over one year (62.5%), while over two years this decreases (to 43.8%). The agreement of two-year changes for HTO patients is low (29.4%) and most patients appear to show more deterioration in CT than in KIDA (64.7%).

Table 3.7: False negatives, false positives and true negatives and positives when comparing the direction of the JSW changes (increase/decrease) for heat maps created from CT images with the JSW change direction in KIDA for the same patients. In the changes over one year from baseline all KJD patients are included, in the changes over two years from baseline all patients from both treatment groups are included.

	Baseline → One Year	Baseline → Two Years	
	KJD	KJD	HTO
True Negatives + Positives	62.5%	43.8%	29.4%
False Negatives	18.8%	37.5%	64.7%
False Positives	18.8%	18.8%	5.9%

As seen in table 3.8, the change in total WOMAC score has a better agreement in classification with KIDA (76.0%) than with CT (28.0%). The total WOMAC score improved for all patients while the VAS score improved for all but two patients. Like WOMAC, the change in VAS over two years has a better agreement with KIDA (67.9%) than CT (42.9%).

Table 3.8: Agreement of KIDA mean joint value change direction (increase/decrease) and direction of change in heat maps from CT images (improvement/deterioration) with the clinical parameter change direction (improvement/deterioration in VAS score or total WOMAC score).

	Δ KIDA (Mean Joint)	Δ CT (Heat Maps)
Δ VAS	67.9%	42.9%
Δ WOMAC total	76.0%	28.0%

3.4 Minor confounders

With linear regression, the influence of minor confounders on the relation between KIDA and 3D CT JSW was tested for both patient groups and both sides of the joint, on absolute JSW values (baseline, one year and two years together) and on two-year delta values. For each relation, all possible confounders were included in the model and the one with the highest p-value was removed until a statistically significant model remained with only statistically significant confounders. Groups of confounders were found that made the correlations between KIDA and CT stronger and more significant, but these confounders were not consistent for both sides of the joint and for both patient groups and could therefore not explain the non-significant correlation in delta values. When evaluating these relations, it was hypothesized that the statistically significant correlation might be due to the effect of outliers in a relatively small population and it was decided that there are no minor confounders that could explain the differences in delta values for KIDA and CT.

3.5 Explorative MRI study: The effect of weight-bearing and knee flexion on the joint space

General pattern changes are described as seen for all participants, using representative JSW distribution images to describe the changes.

3.5.1 Flexion

Pattern changes as a result of flexion while weight-bearing can be seen in figure 3.1, where the top two images show the heat maps for the extended and flexed (30°) position while weight-bearing. Figure 3.1C displays a contrast heat map of the difference between the two positions. The blue color indicates locations where the distances increase when flexing while the red color indicates locations where they decrease with respect to the extended position.

As seen in figure 3.1C, flexing while weight-bearing shows a clear pattern change, with the joint space distances becoming smaller posteriorly and bigger anteriorly. The histograms in figure 3.1D show the main peak for smaller distances does not change greatly, though the peak for the flexed position is positioned slightly more to the right. In non-weight-bearing position, the contrast heat map shows the same shift to the anterior direction when flexing. The histogram indicates no real differences in the main peaks.

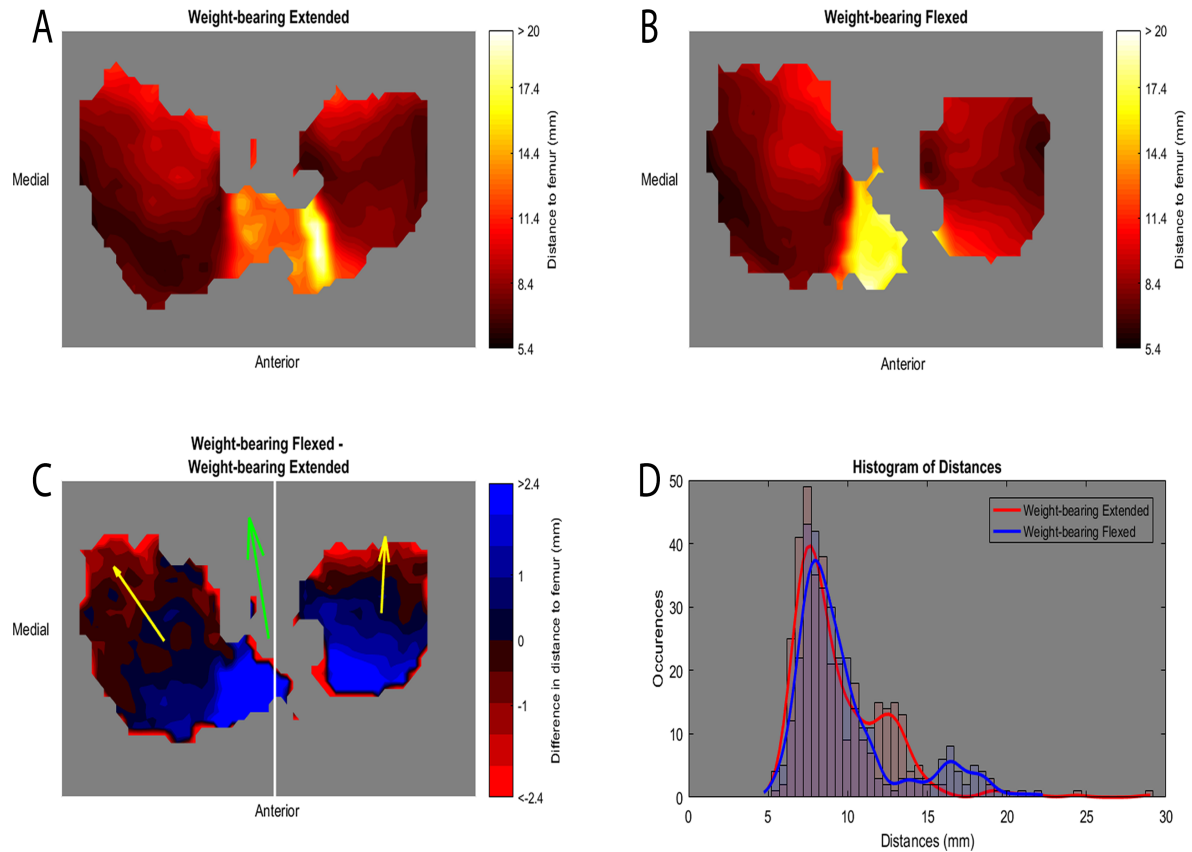


Figure 3.1: Joint space changes when changing position from weight-bearing extended to weight-bearing flexed for the first volunteer. The top two figures show the different heat maps for the extended (A) and flexed (B) position. (C) shows a heat map of the differences between (A) and (B), with blue indicating places where distances are bigger for the flexed position and red indicating where distances are smaller for the flexed position. The arrows show the direction of change for the whole joint (green) and both sides separated (yellow) as indicated by the white line. (D) shows a histogram of the distances for both positions.

3.5.2 Weight-bearing

Pattern changes as a result of weight-bearing while the leg is extended can be seen in figure 3.2. The contrast heat map does not show a clear pattern change between weight-bearing and non-weight-bearing, while the histogram shows a slightly higher main peak, meaning that there are more smaller distances when weight-bearing as opposed to non-weight-bearing. In a flexed position, the contrast heat map indicates the joint space distances are generally bigger for the non-weight-bearing heat map, as do the histograms. Despite a median joint JSW increase when weight-bearing with respect to non-weight-bearing, the amount of perpendiculars almost did not change.

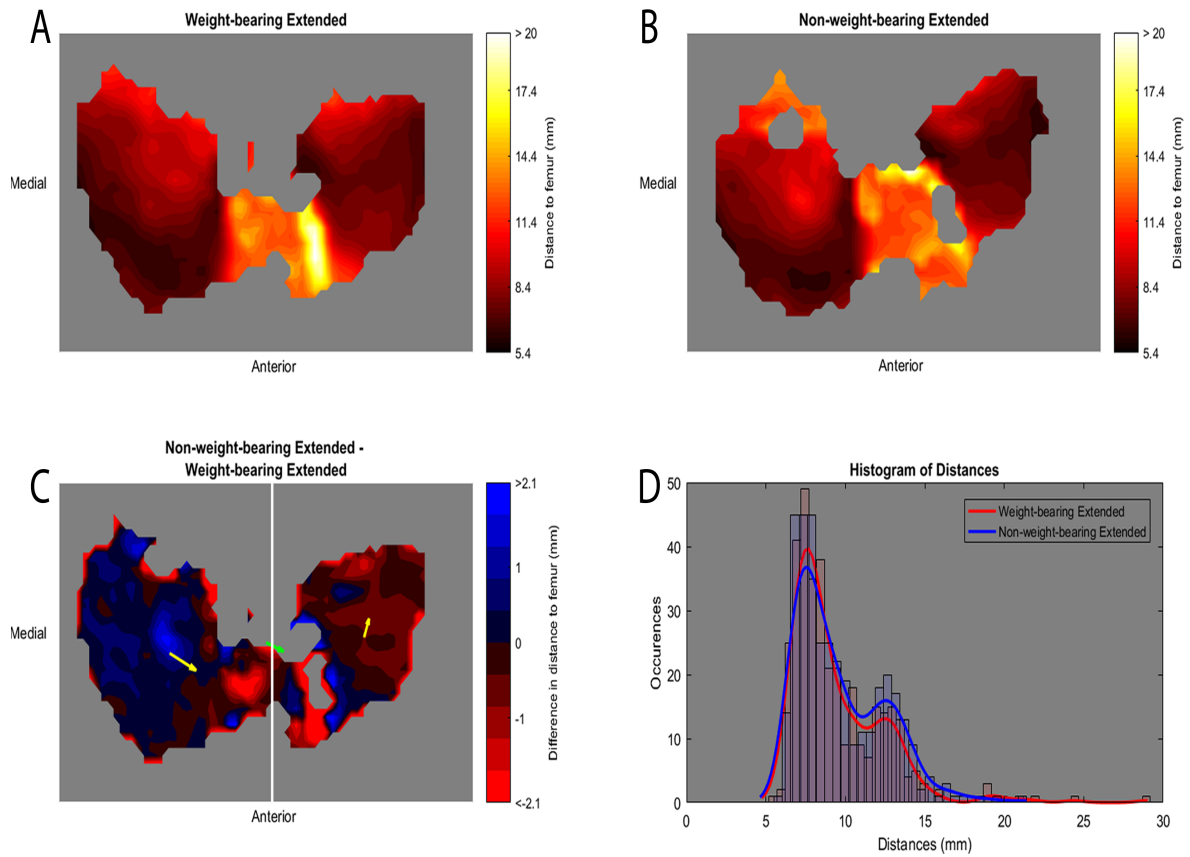


Figure 3.2: Joint space changes when changing position from weight-bearing extended to non-weight-bearing extended for the first volunteer. The top two figures show the different heat maps for the extended (A) and flexed (B) position. (C) shows a heat map of the differences between (A) and (B), with blue indicating places where distances are bigger for the non-weight-bearing position and red indicating where distances are smaller for the non-weight-bearing position. The arrows show the direction of change for the whole joint (green) and both sides separated (yellow) as indicated by the white line. (D) shows a histogram of the distances for both positions.

3.5.3 Radiograph position compared to CT position

When changing from the non-weight-bearing extended position as used in CT and MRI images to the weight-bearing flexed position as used in radiographs, a shift of smaller distances to the posterior position is seen for both sides of the joint. More small distances are present in the weight-bearing flexed position.

Discussion & Conclusion

In this study, a novel 3D joint space quantification method for the evaluation of 3D images of osteoarthritic knees has been explored and described. The technique uses perpendicular lines from the tibia plateau to measure distances to the femur and perpendicular lines from the femur to the tibia to ensure only relevant parts of the joint, involved in a force transfer between the tibia and femur, are included in the joint space. Medial and lateral JSW medians were calculated from CT images and compared with the gold standard, radiography, analyzed with KIDA. Two different patient groups were used: patients treated with KJD and with HTO, treatments anticipated to result in an improved JSW according to literature. Comparing the demographics at baseline between these two treatment groups, KJD patients had statistically significantly higher age and Kellgren-Lawrence score. Part of the KJD patients were included from a trial comparing KJD with TKP, while all HTO patients were included from the trial comparing HTO with KJD. TKP is typically performed in later stage OA, potentially explaining the found differences.

The algorithm developed to calculate the joint space distances in 3D was chosen to be semi-automatic. A balance was found between using a fast but less precise automatic method and a slow but precise manual method. Automatic methods require less time than manual methods and require no input from the user, decreasing inter- and intra-user variability. However, allowing less choice by the user also means mistakes made by the program cannot be easily corrected. Automatic methods will not necessarily work on all patients, since not every small variation between patients can always be taken into account by the program. For example, differences in subchondral bone density and thus image intensity make it difficult to develop one method that can detect bone edges for both high and low intensity bone, especially since intensities seem to change between patients and within the joint of a single patient. For these reasons, the choice was made for a semi-automatic method, combining an automatic program with user input to adjust the program's initial segmentation. Additionally, the bone segmented from the different slices was smoothed to remove surface irregularities that may have been caused by the imaging method because of pixel size and slice thickness limitations. A smoothed reconstruction should correspond with reality better, especially since cartilage is meant to create a smooth surface [3]. Smoothing too much could result in an unrealistically smooth surface that alters the entire bone shape, so the optimal amount of smoothing was determined visually. Perpendiculars were averaged over a predetermined grid to further ensure correct representation of the local bone surface. For more discussion and consideration on different choices in the algorithm development, see Appendix A.

The semi-automatic method is still rather fast, taking an average of 4 minutes from loading the 3D CT scan to having the results displayed, compared to around 30 seconds for a method that is fully automatic but more prone to errors. Furthermore, the developed method works on all scans tested and on both CT and MRI images. A 3D imaging technique and calculation method can display the joint space width distribution throughout the joint, which was done with heat maps. The reconstructed bones can be used to calculate the JSW in 2D, similar to KIDA, and to express measurement results in more objectively comparable numbers, the median JSW of the medial and lateral side of the joint can be calculated.

To validate these median 3D measurement results, they were compared with the gold standard radiography, measured with KIDA. In both patient groups, KIDA medial and lateral JSW showed a significant positive cross-sectional correlation with 3D CT that was moderate to strong. For this cross-sectional analysis, the JSW values on baseline (before treatment) and one and two years after treatment were used. Comparing group JSW means, it was seen that 2D CT JSW means are always lower than 3D CT JSW means. This is expected, since in 2D CT the measurement method in KIDA is simulated, where distances are measured between the lower part of the femur and the frontal ridge of the tibia. These parts of the tibia are in reality not positioned above each other and should be closer together than parts of the joint that are actually positioned above each other, such as the lower part of the femur and the lower, central part of the medial and lateral side of the tibia. For this reason, KIDA mean results were also expected to be lower than 3D CT, and slightly lower than 2D CT because of the effect of weight-bearing. This was true for the medial side of the joint, but for the lateral side of the joint KIDA means were higher than both 3D and 2D CT. This cannot be directly explained from the available data. It could be that the flexed position in KIDA puts more pressure on the medial side of the joint while relieving the lateral side and thus increasing the lateral JSW, or that the weight-bearing causes the most affected, medial, side to be more compressed, resulting in a slight axis change that increases the lateral JSW only when weight-bearing.

Since cross-sectional correlations were so strong, good correlations were expected longitudinally as well. However, most of the strong and statistically significant correlations disappeared when looking at the two-year delta scores. For KIDA JSW correlations with 3D CT, only the lateral side in KJD patients remained statistically significant.

The mean changes for both sides of the joint and both patient groups when measuring with KIDA or with 2D or 3D CT were compared to possibly explain the lack of statistical significance. This showed that KIDA and 3D CT only showed change direction agreement for the lateral side in KJD patients, which is the same side and group that showed a good Pearson correlation, so these mean changes did not provide more insight in the differences between KIDA and CT.

A paired samples t-test for the medial and lateral changes over two years as measured by KIDA and 3D CT was performed to analyze how significant the two-year changes were. While for the KJD patients both sides of the joint at least show a change in the same direction for KIDA and CT, even if they are not always significant, the medial side in HTO patients shows a significant change in opposite direction. Since the medial KIDA JSW is significantly increasing and the medial 3D CT JSW significantly decreasing, it is logical that there is no correlation found between the two. It is still not explained, however, why the techniques show an opposite change.

It was hypothesized that perhaps expressing the 3D CT in medial and lateral median JSW is not the optimal method and is not able to express changes well. Therefore, the heat maps were visually scored for improvement or deterioration over time and this change direction was compared to the change direction in KIDA mean joint JSW. These changes correlated slightly better for patients treated with KJD, but the correlation for HTO patients remained low, so it seems that the reason for the weak longitudinal correlations should not be sought in different ways of expressing CT JSW.

Perhaps the gold standard that the CT JSW changes are compared to is not optimal. The CT measurements are compared to radiology since it is the gold standard, and in the Rheumatology department of the UMC Utrecht KIDA is additionally used for JSW measurements, but this does not mean it gives perfect joint space width measurement results. Both KIDA and CT JSW changes over time were compared to the change in clinical parameters (WOMAC and VAS) to see if perhaps CT correlated better with clinical parameters, but it was seen that KIDA showed more agreement with the change in WOMAC and VAS. It should be noted that, as stated before, the clinical parameters improve over time for nearly all patients and an increase in WOMAC or VAS is not necessarily the result of cartilage regeneration or JSW increase, but also because patients learn to cope with their disease better [75]. Furthermore, the two patients that showed a deterioration in clinical parameters did not show a deterioration in KIDA, while they did show a deterioration in the CT heat maps. Still, KIDA correlated better with clinical parameters, so it was tried further to find an explanation for the bad longitudinal correlation between KIDA and CT and perhaps the reason could be the influence of minor confounders.

Linear regression was used to test for minor confounders, since perhaps these could explain the unexpected findings, as found in literature. However, as mentioned in the results section, there was

no confounder or group of confounders that had a significant influence on both sides of the joint. Therefore, none of the available demographic data can explain the significant differences in changes over time that are seen especially in HTO patients.

The fact that longitudinal correlation between KIDA and the 2D over-projection CT, aimed to measure the JSW similarly to KIDA while using CT images, was weak as well indicates the difference in change over time does not rise from the different JSW calculation methods, but from the difference in weight-bearing and knee flexion. As has been mentioned before, Kan et al [52] proved a semi-flexed weight-bearing position causes significantly smaller JSW measurements in radiographs with respect to an extended weight-bearing position, so even in radiographs leg position has a clear effect on measurement results. KIDA more often shows an increase over time than CT and a possible explanation could be that unhealthy cartilage depresses more while weight-bearing than healthy cartilage does, while this effect is not seen as clearly on non-weight-bearing images if the total cartilage volume remains similar. A treatment that regenerates unhealthy cartilage would then cause a JSW increase on radiographs but not (as much) on CT. Another possibility is that when measuring JSW not just the effect of cartilage change is incorporated, but the effect of ligaments, muscles and menisci as well. Especially factors such as meniscal extrusion, which is related to OA [76, 77], could have different effects while weight-bearing and flexed than while non-weight-bearing and extended. It could be that all these non-cartilage related factors result in more JSW when non-weight-bearing, further increased by the fact that OA joints contain more fluid that could fill the joint space while non-weight-bearing. A treatment that has a positive effect on OA could cause almost no JSW change in CT, since even if cartilage regeneration causes a JSW increase, the JSW increasing effect of the other factors is decreased. This could explain the fact that the paired samples t-test showed a significant medial increase in KJD patients while measuring with KIDA but not while measuring with CT.

It could also be that KIDA correlates better with clinical parameters because it measures more specifically the smaller distances because of the position in which the radiographs are taken. Both flexion and weight-bearing seem to cause smaller distances, and the fact that the KIDA mean lateral JSW is almost unrealistically high indicates perhaps the radiograph position even deliberately shifts the weight and thus smaller distances to the medial side of the joint. Measuring in a position that causes smaller joint space distances could explain a better correlation with clinical parameters, since lack of joint space is what causes the most pain and discomfort in OA patients.

The possible influence of flexion and weight-bearing, the major confounders in this research, was investigated with an MRI experiment with healthy volunteers. It was observed that flexion of the knee causes a shift of smaller distances in posterior direction compared to extension while weight-bearing causes generally smaller distances compared to non-weight-bearing. Changing from a non-weight-bearing extended leg to a weight-bearing flexed leg, so comparing the CT or MRI position to the radiography position, causes smaller distances throughout the entire joint as well as a shift of smaller distances to the posterior side of the joint. These changes were found in the healthy volunteers, but the findings could be different in OA patients either untreated or treated with an HTO or KJD. However, the fact that the healthy volunteers all showed a clear difference in joint space distances as well as the location of smaller joint space distances in the joint indicates that this is the right path to eventually explain the difference in two-year JSW changes in KIDA and CT.

Clearly this is a first step and explorative research. Further research in a larger relevant population is necessary to investigate these possible explanations. It would be interesting to repeat the MRI experiment as described in this research, scanning OA patients as well as age-matched healthy volunteers. This could lead to more understanding about the behavior of damaged cartilage in weight-bearing or even flexing situations compared to healthy cartilage. Furthermore, HTO patients could be included in the experiment, which could provide more information about the leg axis change after an HTO and how this affects both the weight-bearing and non-weight-bearing situation. The results of such an experiment would give additional insight into osteoarthritic joint space changes when weight-bearing and flexing. In order to more objectively define which JSW measurement method relates best to the cartilage change, MRI data of the same patients that are measured with both KIDA and the CT method could be used to perform qualitative and quantitative cartilage measurements. MRI scans that could be used for this include quantitative sequences like PDW or Eckstein, and qualitative sequences like T2-mapping or dGEMRIC protocols. It is possible that some adjustments to the semi-automatic

method should be made to optimally represent the 3D joint space. The possibility to filter perpendiculars based on the angle between the perpendicular from the femur and the matching perpendicular from the femur to the tibia has not been explored in this research. Applying an angle limit could give a better representation of joint space area involved in the force transfer between the tibia and femur. With an angle limit of 25 degrees, for example, many large and possibly less relevant joint space distances are removed, while many smaller distances are preserved. More research should be done into what angle limit results in a clinically relevant joint space. Furthermore, the perpendiculars as calculated from the CT scans could be filtered more specifically to include only parts of the tibia plateau where weight-bearing cartilage is usually present. Especially the intercondylar area of the tibia is now included in the heat maps and though a significant part of it is removed when separating the perpendiculars in the medial and lateral side, this filtering could be done more specifically to include only the condylar medial and lateral area. This would have to be done manually and it would be interesting to see how this affects measurements in future research. The fact that the amount of perpendiculars that is left after filtering does not significantly change between the weight-bearing and non-weight-bearing position even if the median JSW becomes bigger, as seen in the MRI experiment, does indicate that even in non-weight-bearing position the selected perpendiculars are able to represent the force transfer between the femur and tibia well.

This research has explored the possibility of using three-dimensional imaging to quantify the knee joint space. A semi-automatic algorithm has successfully been developed and applied on images of knee osteoarthritis patients before and after two joint-sparing treatments. It has been made possible to visualize the joint space in 3D and automatically generate different joint space width distances. Differences in changes over time between the CT JSW measurements from developed method and the JSW changes in the gold standard KIDA were observed and have been tried to explain in several ways, but so far no definitive explanation has been found. A quantitative proof-of-principle MRI experiment has been performed with healthy volunteers to gain more insight into changes in the joint space when weight-bearing or flexing the knee, as these variables differ between radiography and CT. Since these position changes resulted in clear joint space differences, it is expected these position differences are the right path to understand the differences between CT and KIDA. Several possibilities for future research have been proposed to better relate different measurement methods and gain more insight into what these methods are actually measuring. These additional studies could help determine a way to translate JSW measurements between different positions with the variable of weight-bearing, enabling comparison between different modalities, and eventually making the method applicable in research or clinical setting. The semi-automatic method alone, as it has been developed in this research, is already of additional value next to the gold standard for visualizing the joint space throughout the entire joint.

Bibliography

- [1] F. Lafeber, N.J. Besselink, and S.C. Mastbergen. *Osteoarthritis: synovium and capsule*, chapter 6, page 55. Oxford University Press, 3rd edition.
- [2] J.P. Goldblatt and J.C. Richmond. Anatomy and biomechanics of the knee. *Operatove Techniques in Sports Medicine*, 11(3):172–186, 2003.
- [3] A.J.S. Fox, A. Bedi, and S.A. Rodeo. The basic science of articular cartilage. *Sports Health*, 1(6):461–468, 2009.
- [4] I. Shrier. Muscle dysfunction versus wear and tear as a cause of exercise related osteoarthritis: an epidemiological update. *Br J Sports Med*, 38(5):526–535, 2004.
- [5] R.L. Drake, W. Vogl, and A.W.M. Mitchell. *Gray’s Basic Anatomy*. Elsevier Health Sciences, 2012.
- [6] J.Y. Reginster. The prevalence and burden of arthritis. *Rheumatology*, 41(1):3–6, 2002.
- [7] J.W.J. Bijlsma and K. Knahr. Strategies for the prevention and management of osteoarthritis of the hip and knee. *Best Pract Res Clin Rheumatol*, 21(1):59–76, 2007.
- [8] J.A. Buckwalter and J.A. Martin. Osteoarthritis. *Adv Drug Deliv Rev*, 58(2):150–167, 2006.
- [9] L.S. Simon. Osteoarthritis: A review. *Clinical Cornerstone*, 2(2):26–37, 1999.
- [10] D.J. Hunter and D.T. Felson. Osteoarthritis. *BMJ*, 332(7542):639–642, 2006.
- [11] J.Y. Reginster. The prevalence and burden of arthritis. *Rheumatology*, 41(1):3–6, 2002.
- [12] L.S. Lohmander, M. Gerhardsson de Verdier, J. Rollof, P.M. Nilsson, and G. Engstrom. Incidence of severe knee and hip osteoarthritis in relation to different measures of body mass: a population-based prospective cohort study. *Ann Rheum Dis*, 68(4):490–496, 2009.
- [13] V.K. Srikanth, J.L. Fryer, G. Zhai, T.M. Winzenberg, D. Hosmer, and G. Jones. A meta-analysis of sex differences prevalence, incidence and severity of osteoarthritis. *Osteoarthritis Cartilage*, 13(9):769–781, 2005.
- [14] R.L. Neame, K. Muir, S. Doherty, and M. Doherty. Prevalence of knee osteoarthritis in the United States: arthritis data from the Third National Health and Nutrition Examination Survey 1991-94. *J Rheumatol*, 33(11):2271–2279, 2006.
- [15] D.T. Felson, Y. Zhang, M.T. Hannan, A. Naimark, B. Weissman, P. Aliabadi, and D. Levy. Risk factors for incident radiographic knee osteoarthritis in the elderly. the Framingham study. *Arthritis Rheum*, 40(4):728–733, 1997.
- [16] R.L. Neame, K. Muir, S. Doherty, and M. Doherty. Genetic risk of knee osteoarthritis: a sibling study. *Ann Rheum Dis*, 63(9):1022–1027, 2004.
- [17] C. Cooper, S. Snow, T.E. McAlindon, S. Kellingray, B. Stuart, D. Coggon, and P.A. Dieppe. Risk factors for the incidence and progression of radiographic knee osteoarthritis. *Arthritis Rheum*, 43(5):995–1000, 2000.
- [18] F. Cicuttini, A. Wluka, J. Hankin, and Y. Wang. Longitudinal study of the relationship between knee angle and tibiofemoral cartilage volume in subjects with knee osteoarthritis. *Rheumatology (Oxford)*, 43(3):321–324, 2004.
- [19] G.M. Brouwer, A.W. van Tol, A.P. Bergink, J.N. Belo, R.M. Bernsen, M. Reijman, H.A. Pols, and S.M. Bierma-Zeinstra. Association between valgus and varus alignment and the development and progression of radiographic osteoarthritis of the knee. *Arthritis Rheum*, 56(4):1204–1211, 2007.
- [20] Y. Zhang and J.M. Jordan. Epidemiology of Osteoarthritis. *Clin Geriatr Med*, 26(3):355–369, 2010.
- [21] Reumafonds. Artrose, Over de ziekte, Diagnose.

- [22] W. Zhang, M. Doherty, G. Peat, M.A. Bierma-Zeinstra, N.K. Arden, B. Breshihan, G. Herrero-Beaumont, S. Kirschner, B.F. Leeb, L.S. Lohmander, B. Mazières, K. Pavelka, A.K. So, T. Tuncer, I. Watt, and J.W. Bijlsma. EULAR evidence-based recommendations for the diagnosis of knee osteoarthritis. *Ann Rheum Dis*, 69(3):483–489, 2010.
- [23] G. Sakellariou, P.G. Conaghan, W. Zhang, J.W.J. Bijlsma, P. Boyesen, M.A. D’Agostino, M. Doherty, D. Fodor, M. Kloppenburg, F. Miese, E. Naredo, M. Porcheret, and A. Iagnocco. EULAR recommendations for the use of imaging in the clinical management of peripheral joint osteoarthritis. *Ann Rheum Dis*, 76(9):1484–1494, 2017.
- [24] F.W. Roemer, M.D. Crema, S. Trattnig, and A. Guermazi. Advances in Imaging of Osteoarthritis and Cartilage. *Radiology*, 260(2):332–354, 2011.
- [25] H.J. Braun and G.E. Gold. Diagnosis of osteoarthritis: Imaging. *Bone*, 51(2):278–288, 2012.
- [26] J.C. Buckland-Wright, D.G. Macfarlane, J.A. Lynch, M.K. Jasani, and C.R. Bradshaw. Joint space width measures cartilage thickness in osteoarthritis of the knee: high resolution plain film and double contrast macroradiographic investigation. *Annals of the Rheumatic Diseases*, 54:263–268, 1995.
- [27] S.R. Oak, A. Ghodadra, C.S. Winalski, A. Miniaci, and M.H. Jones. Radiographic joint space width is correlated with 4-year clinical outcomes in patients with knee osteoarthritis: data from the osteoarthritis initiative. *Osteoarthritis and Cartilage*, 21:1185–1190, 2013.
- [28] J.H. Kellgren and J.S. Lawrence. Radiological Assessment of Osteo-Arthrosis. *Ann Rheum Dis*, 16(4):494–502, 1957.
- [29] R.D. Altman and G.E. Gold. Atlas of individual radiographic features in osteoarthritis, revised. *Osteoarthritis Cartilage*, 15(Suppl A):A1–A56, 2007.
- [30] J.P. Pelletier, C. Cooper, J.Y. Reginster, O. Bruyère, R. Chapurlat, F. Cicuttini, P.G. Conaghan, M. Doherty, H. Genant, G. Giacobelli, M.C. Hochberg, D.J. Hunter, J.A. Kanis, M. Kloppenburg, J.D. Laredo, T. McAlindon, M. Nevitt, J.P. Raynauld, R. Rizzoli, C. Zilkens, F.W. Roemer, J. Martel-Pelletier, and A. Guermazi. What is the predictive value of MRI for the occurrence of knee replacement surgery in knee osteoarthritis? *Ann Rheum Dis*, 72(10):1594–1604, 2013.
- [31] A.D. Beswick, V. Wylde, R. Gooberman-Hill, A. Blom, and P. Dieppe. What proportion of patients report long-term pain after total hip or knee replacement for osteoarthritis? a systematic review of prospective studies in unselected patients. *BMJ Open*, 2(1), 2012.
- [32] A.M. Weinstein, B.N. Rome, W.M. Reichmann, J.E. Collins, S.A. Burbine, T.S. Thornhill, J. Wright, J.N. Katz, and E. Losina. Estimating the burden of total knee replacement in the United States. *J Bone Joint Surg Am*, 95(5):385–392, 2013.
- [33] S.M. Javad Mortazavi, J. Molligan, M.S. Austin, M.S. Austin, J.J. Purtill, W.J. Hozack, and J. Parvizi. Failure following revision total knee arthroplasty: infection is the major cause. *Int Orthop*, 35(8):1157–1164, 2011.
- [34] Mayo Clinic Staff. Osteoarthritis Self-management.
- [35] M. Wolcott, S. Traub, and C. Efirid. High tibial osteotomies in the young active patient. *International Orthopaedics*, 34:161–166, 2010.
- [36] M. Denti, P. Volpi, and G. Puddu. *European Instructional Lectures: Volume 13, 2013, 14th EFORT Congress, Istanbul, Turkey*, chapter Modern Indications for High Tibial Osteotomy, pages 253–258. Springer Berlin Heidelberg, 2013.
- [37] K. Wiegant, P.M. van Roermund, F. Intema, S. Cotofana, F. Eckstein, S.C. Mastbergen, and F.P.J.G. Lafeber. Sustained clinical and structural benefit after joint distraction in the treatment of severe knee osteoarthritis. *Osteoarthritis and Cartilage*, 21:1660–1667, 2013.
- [38] K. Wiegant, P.M. van Roermund, F. Intema, S. Cotofana, F. Eckstein, S.C. Mastbergen, and F.P. Lafeber. Sustained clinical and structural benefit after joint distraction in the treatment of severe knee osteoarthritis. *Osteoarthritis Cartilage*, 21(11):1660–1667, 2013.
- [39] J.A.D. van der Woude, K. Wiegant, P.M. van Roermund, F. Intema, R.J.H. Custers, F. Eckstein, J.M. van Laar, S.C. Mastbergen, and F.P.J.G. Lafeber. Five-year follow-up of knee joint distraction; clinical benefit and cartilaginous tissue repair in an open uncontrolled prospective study. *Cartilage*, 8(3):263–271, 2017.
- [40] J. A. D. van der Woude, K. Wiegant, R. J. van Heerwaarden, S. Spruijt, P. M. van Roermund, R. J. H. Custers, S. C. Mastbergen, and F. P. J. G. Lafeber. Knee joint distraction compared with high tibial osteotomy: a randomized controlled trial. *Knee Surg Sports Traumatol Arthrosc*, 25(3):876–886, 2017.

- [41] J. Li, Z. Zhong, R. Lidtke, K.E. Keuttner, C. Peterfy, E. Aliyeva, and C. Muehleman. Radiography of soft tissue of the foot and ankle with diffraction enhanced imaging. *J Anat*, 202(5):463–470, 2003.
- [42] R. Rubin and D.S. Strayer. *Rubin's Pathology 5th edition*. Lippincott Williams And Wilkins, 2007.
- [43] K.A. Beattie, J. Duryea, M. Pui, J. O'Neill, P. Boulos, C.E. Webber, F. Eckstein, and J.D. Adachi. Minimum joint space width and tibial cartilage morphology in the knees of healthy individuals: A cross-sectional study. *BMC Musculoskelet Disord*, 9:119, 2008.
- [44] R.J. Ward, J.C. Buckland-Wright, and F. Wolfe. Relationships between tibial rim alignment and joint space width measurement reproducibility in non-fluoroscopic radiographs of osteoarthritic knees. *Osteoarthritis Cartilage*, 13(11):945–952, 2005.
- [45] N. Yamanaka, T. Takahashi, N. Ichikawa, and H. Yamamoto. Posterior-anterior weight-bearing radiograph in 15 degree knee flexion in medial osteoarthritis. *Skeletal Radiol*, 32(1):28–34, 2003.
- [46] P. Ravaud, G.-R. Auleley, C. Chastang, B. Rousselin, L. Paolozzi, B. Amor, and M. Dougados. Knee joint space width measurement: An experimental study of the influence of radiographic procedure and joint positioning. *British Journal of Rheumatology*, 35:761–766, 1996.
- [47] B.K. Paunipagar and D.D. Rasalkar. Imaging of articular cartilage. *Indian J Radiol Imaging*, 24(3):237–248, 2014.
- [48] I. Möller, D. Bong, E. Naredo, E. Filippucci, I. Carrasco, C. Moragues, and A. Iagnocco. Ultrasound in the study and monitoring of osteoarthritis. *Osteoarthritis Cartilage*, 16(3):S4–7, 2008.
- [49] A. Iagnocco. Imaging the joint in osteoarthritis: a place for ultrasound? *Best Pract Res Clin Rheumatol*, 24(1):27–38, 2010.
- [50] A. Guermazi, D. Hayashi, F. Eckstein, D.J. Hunter, J. Duryea, and F.W. Roemer. Imaging of osteoarthritis. *Rheum Dis Clin N Am*, 39(1):67–105, 2013.
- [51] K. Bevers, J.W. Bijlsma, J.E. Vriezekolk, C.H. van den Ende, and A.A. den Broeder. Ultrasonographic features in symptomatic osteoarthritis of the knee and relation with pain. *Rheumatology (Oxford)*, 53(9):1625–1629, 2014.
- [52] H. Kan, Y. Arai, M. Kobayashi, S. Nakagawa, H. Inoue, M. Hino, S. Komaki, K. Ikoma, K. Ueshima, H. Fujiwara, and T. Kubo. Radiographic measurement of joint space width using the fixed flexion view in 1,102 knees of Japanese patients with osteoarthritis in comparison with the standing extended view. *Knee Surg Relat Res*, 29(1):63–68, 2017.
- [53] A.C.A. Marijnissen, K.L. Vincken, P.A.J.M. Vos, D.B.F. Saris, M.A. Viergever, J.W.J. Bijlsma, L.W. Bartels, and F.P.J.G. Lafeber. Knee Images Digital Analysis (KIDA): a novel method to quantify individual radiographic features of knee osteoarthritis in detail. *Osteoarthritis and Cartilage*, 16(2):234–243, 2008.
- [54] M.H. Merchant Jr, S.C. Willimon, E. Vinson, R. Pietrobon, W.E. Garrett, and L.D. Higgins. Comparison of plain radiography, computed tomography, and magnetic resonance imaging in the evaluation of bone tunnel widening after anterior cruciate ligament reconstruction. *Knee Surg Sports Traumatol Arthrosc*, 18(8):1059–1064, 2010.
- [55] M. Piperno, M.-P.H. Le Graverand, T. Conrozier, M. Bochu, P. Mathieu, and E. Vignon. Quantitative evaluation of joint space width in femorotibial osteoarthritis: comparison of three radiographic views. *Osteoarthritis and Cartilage*, 6:252–259, 1998.
- [56] J.C. Buckland-Wright. Radiographic assessment of osteoarthritis: comparison between existing methodologies. *Osteoarthritis Cartilage*, 7(4):430–433, 1999.
- [57] Staff News Brief. AAOS 2016: Ultra-Low Dose CT Scans Successfully Detect Fractures. *Appl Radiol*, 2016.
- [58] F. Agnesi, K.K. Amrami, C.A. Frigo, and K.R. Kaufman. Semiautomated digital analysis of knee joint space width using MR images. *Skeletal Radiol*, 36(5):437–444, 2007.
- [59] M. Foumani, S.D. Strackee, M. van de Giessen, R. Jonges, L. Blankevoort, and G.J. Streekstra. In-vivo dynamic and static three-dimensional joint space distance maps for assessment of cartilage thickness in the radiocarpal joint. *Clin Biomech*, 28(2):151–156, 2013.
- [60] J.G. Tamez-Pena, A.L. Lerner, J. Yao, A.D. Salo, and S. Totterman. Evaluation of distance maps from fast GRE MRI as a tool to study the knee joint space. *Medical Imaging 2003: Physiology and Function: Methods, Systems, and Applications*, 5031:551–562, 2003.
- [61] E.A. van IJsseldijk, E.R. Valstar, B.C. Stoel, R.G. Nelissen, N. Baka, R. Van't Klooster, and B.L. Kaptein. Three dimensional measurement of minimum joint space width in the knee from stereo radiographs using statistical shape models. *Bone Joint Res*, 5(8):320–327, 2016.

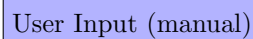
- [62] J. H. Choi, E. J. McWalter, S. Pal, A. Maier, G. E. Gold, and R. Fahrig. Analysis of three-dimensional joint space of the tibiofemoral joint. *2013 IEEE Nuclear Science Symposium and Medical Imaging Conference (2013 NSS/MIC)*, pages 1–4, 2013.
- [63] N.A. Segal, E. Frick, J. Duryea, M.C. Nevitt, J. Niu, J.C. Torner, D.T. Felson, and D.D. Anderson. Comparison of tibiofemoral joint space width measurements from standing CT and fixed flexion radiography. *J Orthop Res*, 35(7):1388–1395, 2017.
- [64] N.A. Segal, E. Frick, J. Duryea, F. Roemer, A. Guermazi, M.C. Nevitt, J.C. Torner, D.T. Felson, and D.D. Anderson. Correlations of medial joint space width on fixed-flexed standing computed tomography and radiographs with cartilage and meniscal morphology on magnetic resonance imaging. *Arthritis Care Res (Hoboken)*, 68(10):1410–1416, 2016.
- [65] D.D. D’Lima, B.J. Fregly, S. Patil, N. Steklov, and C.W. Colwell Jr. Knee joint forces: prediction, measurement, and significance. *Proc Inst Mech Eng H*, 226(2):95–102, 2012.
- [66] J. Parry, D. Antonelli, and W. Ford. Knee joint forces: prediction, measurement, and significance. *J Bone Joint Surg Am*, 57(7):961–967, 1975.
- [67] R. Singerman, J. Berilla, M. Archdeacon, and A. Peyser. In vitro forces in the normal and cruciate-deficient knee during simulated squatting motion. *J Biomech Eng*, 121(2):234–242, 1999.
- [68] D.D. D’Lima, C.P. Townsend, S.W. Arms, B.A. Morris, and C.W. Colwell Jr. An implantable telemetry device to measure intra-articular tibial forces. *J Biomech*, 38(2):299–304, 2005.
- [69] J.A.D. van der Woude, K. Wiegant, R.J. van Heerwaarden, S. Spruijt, P.M. van Roermund, R.J.H. Custers, S.C. Mastbergen, and F.P.J.G. Lafeber. Knee joint distraction compared with high tibial osteotomy: a randomized controlled trial. *Knee Surg Sports Traumatol Arthrosc*, 25(3):876–886, 2017.
- [70] Nederlands Trial Register. Trial Info: Knee joint distraction in comparison with high tibial osteotomy in treatment of knee osteoarthritis.
- [71] Nederlands Trial Register. Trial Info: Knee joint distraction in comparison with total knee prosthesis in treatment of knee osteoarthritis.
- [72] J.C. Buckland-Wright, R.J. Ward, C. Peterfly, C.F. Mojciak, and R.L. Leff. Reproducibility of the semiflexed (metatarsophalangeal) radiographic knee position and automated measurements of medial tibiofemoral joint space width in a multicenter clinical trial of knee osteoarthritis. *J Rheumatol*, 31(8):1588–1597, 2004.
- [73] Esaote S.p.A. European patent application: Method for generating 2D or 3D maps of MRI T1 and T2 relaxation times.
- [74] J. Canny. A computational approach to edge detection. *IEEE Transactions on Pattern Analysis and Machine Intelligence*, PAMI-8(6):679–698, 1986.
- [75] K.N. Alschuler, I.R. Molton, M.P. Jensen, and D.L. Riddle. Prognostic value of coping strategies in a community-based sample of persons with chronic symptomatic knee osteoarthritis. *Pain*, 154(12):2775–2781, 2013.
- [76] M.D. Crema, F.W. Roemer, D.T. Felson, M. Englund, K. Wang, M. Jarraya, M.C. Nevitt, M.D. Marra, J.C. Torner, C.E. Lewis, and A. Guermazi. Factors associated with meniscal extrusion in knees with or at risk for osteoarthritis: The multicenter osteoarthritis study. *Radiology*, 264(2):494–503, 2012.
- [77] J.A. van der Voet, J. Runhaar, P. van der Plas, D. Vroegindewey, E.H. Oei, and S.M.A. Bierma-Zeinstra. Baseline meniscal extrusion associated with incident knee osteoarthritis after 30 months in overweight and obese women. *Osteoarthritis Cartilage*, 25(8):1299–1303, 2017.

Detailed Explanation of Methods

This appendix provides a detailed explanation of several steps as explained in the Methods. First the bone segmentation method is elaborated on with a flow chart, highlighting every step. In a different flow chart, the automatic edge fixing is explained in more technical detail. Lastly, the different choices that were made in this research but have not yet been mentioned in this thesis are highlighted.

A.1 Bone Segmentation

On the next pages, a flow chart displays the process of bone segmentation. Pictures are used to display the different (interim) results and two different nodes either automatic or manual steps:

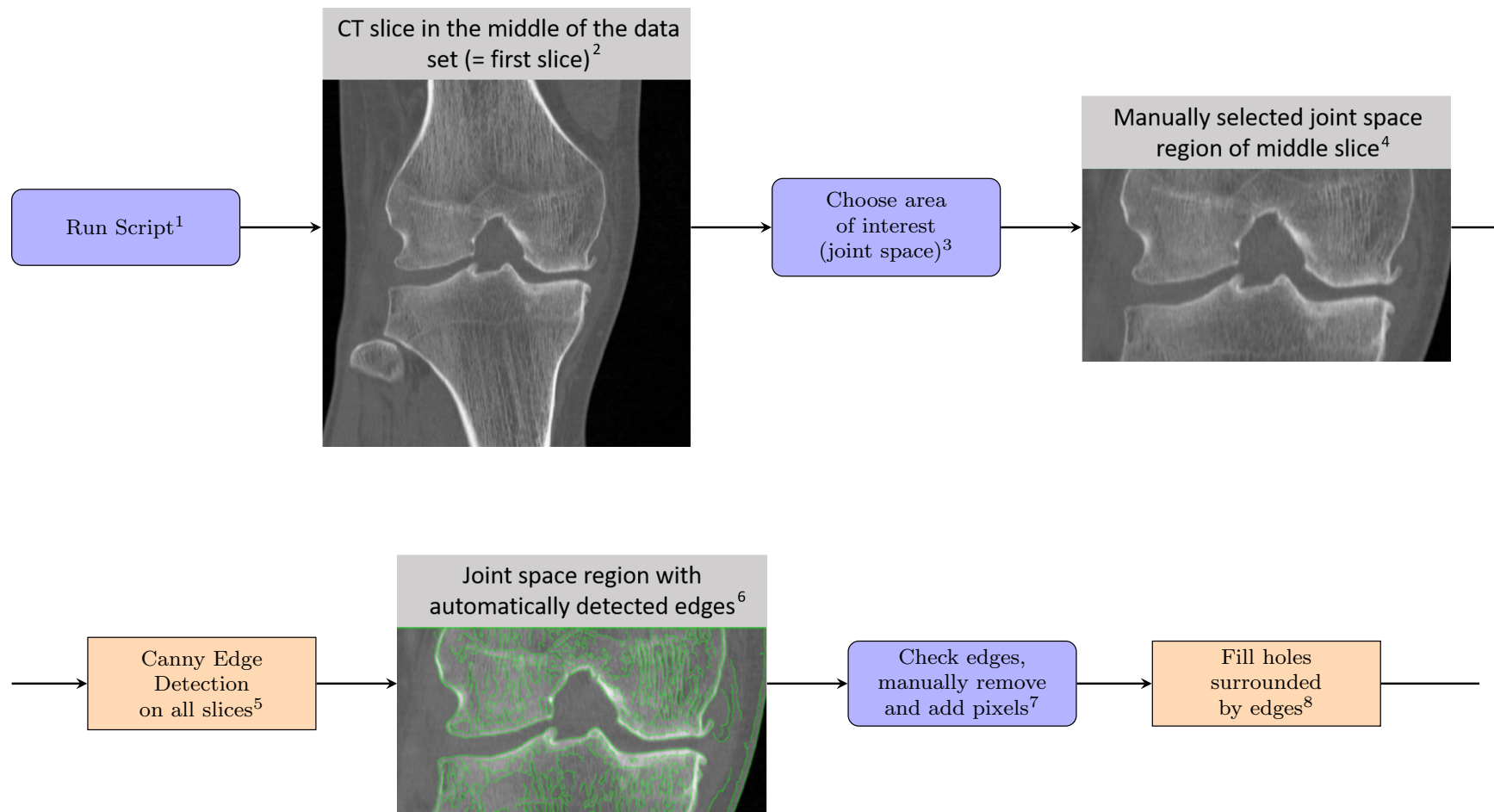


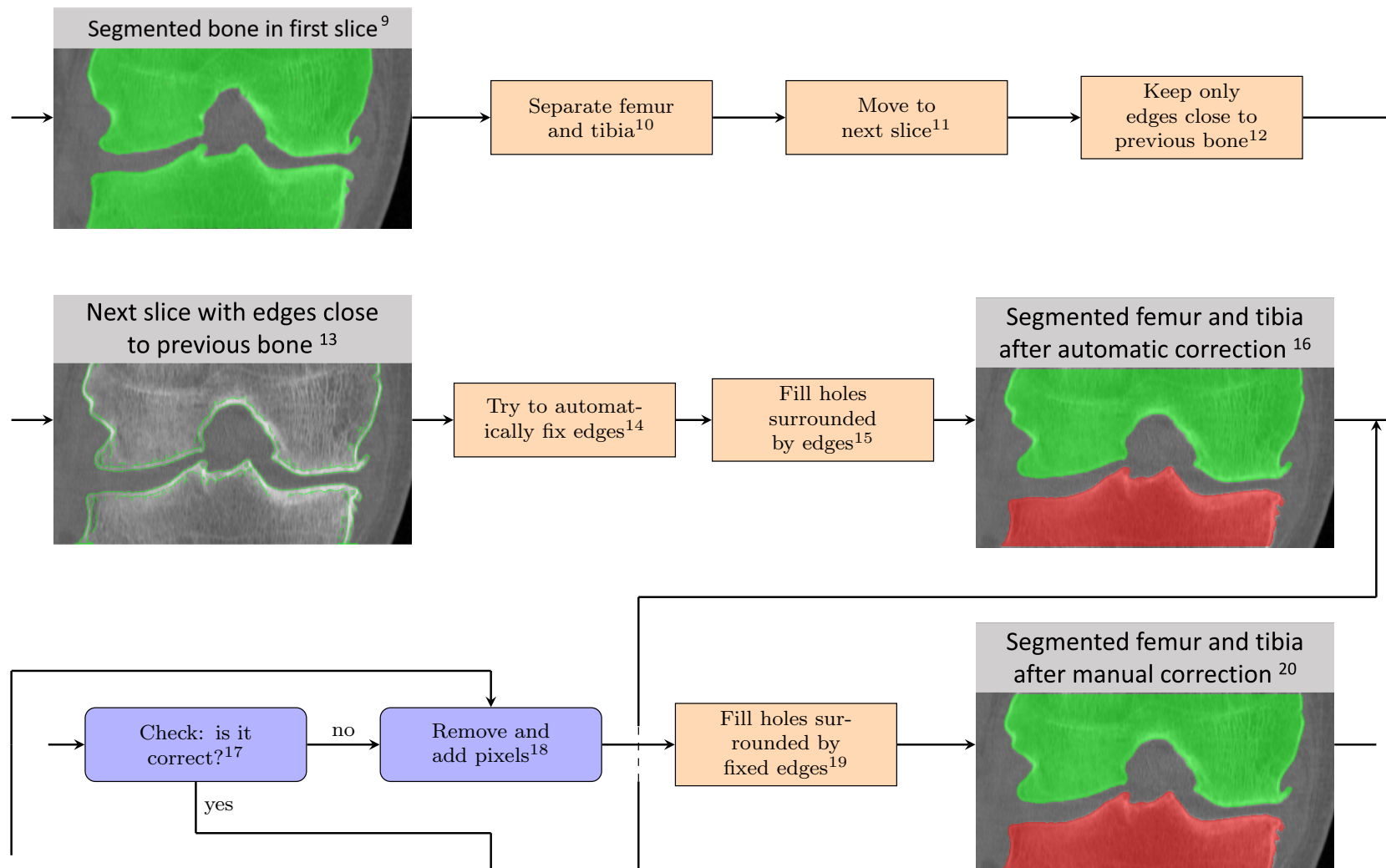
User Input (manual)

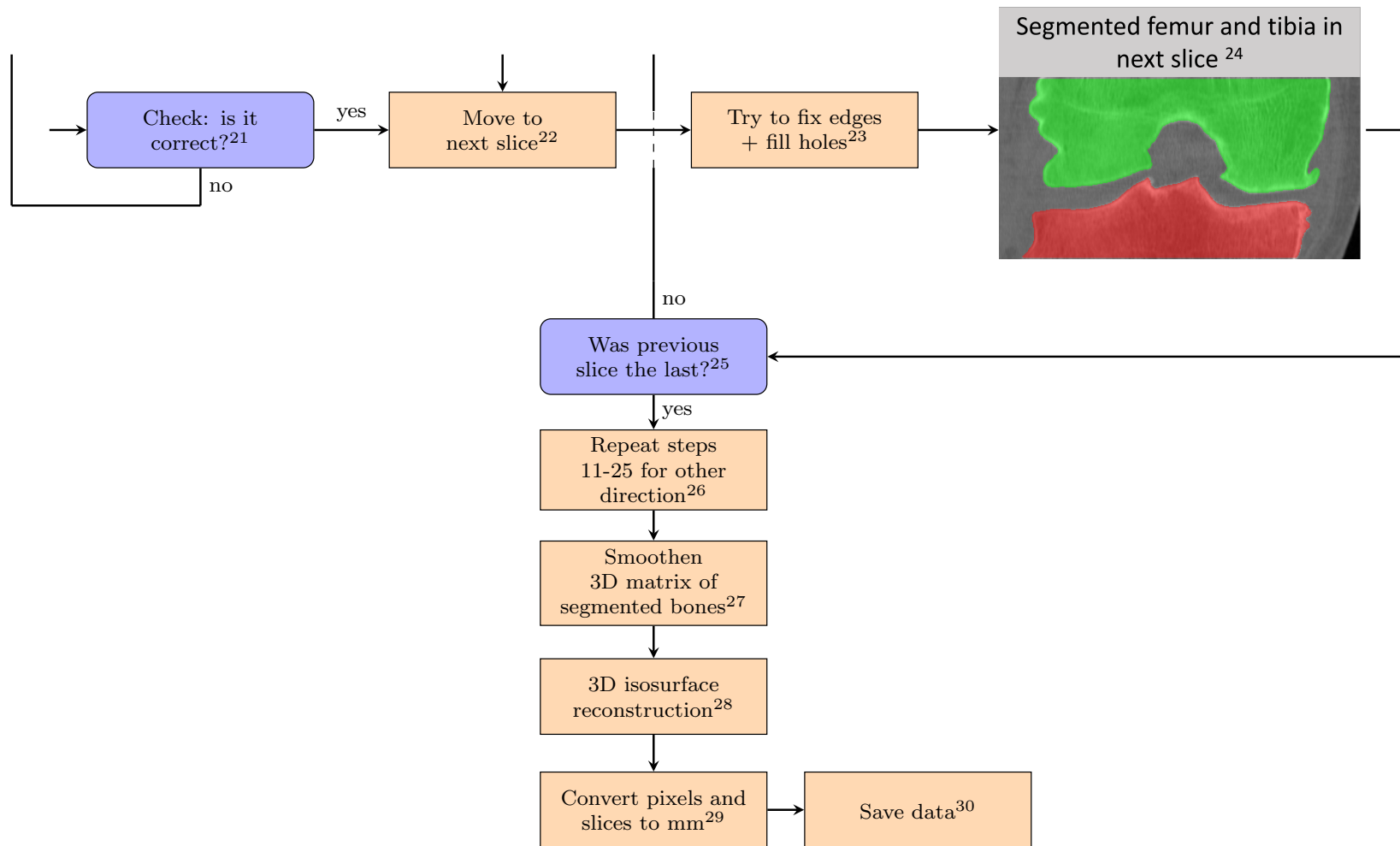


MATLAB Process (automatic)

Every step in the flow chart is numbered and elaborated on more on the pages after the flow chart.





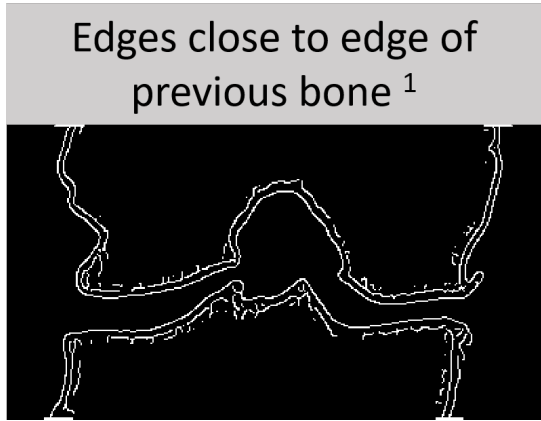


1. The user runs the scripts, providing as input the details of which scan should be analyzed (patient number and time)
2. The middle slice of the scan data is shown, since on many scans this slice is positioned somewhere near the middle of the joint and therefore gives a clearly recognizable overview of the femur and tibia. Optimally, a DICOM viewer is built in, allowing the user to scroll through the entire scan to get an idea of this patient's specific bone anatomy and to choose the best slice to start with.
3. The user draws a rectangle in the first slice to select the joint space area. The data around this rectangle is deleted in all slices, so it should be drawn big enough to allow bone shape changes throughout slices to still be positioned inside the rectangle.
4. The joint space part of the first slice. This is not shown to the user, but is shown in the flow chart to highlight the changes happening.
5. Canny Edge Detection is performed on the joint space area of all slices in the scan. After experimenting with different settings, for CT scans the optimal result was gained when not specifying any settings. For MRI scans this depends on the specific scanning protocol that was used, but these settings can be changed easily if desired.
6. The joint space region of the first slice with the automatically detected edges. Although the bone edges are marked very well, there are usually some holes of a few pixels. Since this is the first slice and thus all detected edges (indirectly) depend on the fact if in this slice the bone is segmented well, no automatic fixing of edges is attempted yet.
7. The detected edges can be fixed by removing or adding pixels. Removing of pixels is done by drawing rectangles in this all marked pixels are removed and adding of pixels is done by marking pairs of pixels between which a line should be drawn. The goal is to have the bones marked by edges without holes and to have no other areas that are completely enclosed by other 'random' edges.
8. Areas that are surrounded by edges are filled. For this reason, the bone edges should contain no holes and should be the only edges completely surrounding an area.
9. If the edges were detected and fixed correctly, filling of holes surrounded by edges should result in perfectly segmented bones, as is the case in the image.
10. The segmented bones are separated in the femur and tibia by determining that the upper group of segmented pixels is the femur and the bottom group is the tibia. In all next slices the separation is done before showing the result by checking which detected groups of pixels match which bone from the previous slice.
11. Since this slice is done, the script moves on to the next slice. This is first done in posterior direction and, after that side of the joint is done, the process is repeated in anterior direction, eventually segmenting the bones throughout the entire joint.
12. Edge detection was performed in the beginning, on all slices. Now, only the pixels of the detected edges that are within 10 pixels distance from the outer line of the bones detected in the previous slice are kept. This way, only detected edges that could actually be bone edges are saved. This makes automatically fixing the edges easier, since many irrelevant or wrongly detected edges are removed. The distance of 10 pixels was chosen after trying many numbers of pixels since the right amount of edges remained. The optimal distance, however, depends on pixel size as well as slice thickness, since the thickness of slices defines the amount of change between slices in structure. Since in CT scans the bone is distinguished relatively easily, 10 pixels works fine even for varying pixel size and slice thickness. In MRI scans, where more soft tissue around the bone is detected with edge detection, the optimal distance should be found before starting segmentation, which is easy to do and should not take much time.
13. The user does not see this image usually, since it is only an interim step that does not require user input.

14. The script tries to automatically fix detected edges. Since this step actually consists of multiple different steps, a more technical explanation can be found later in this appendix under 'Automatic Edge Fixing'.
15. Like before, the areas surrounded by edges are filled.
16. If the automatic detection and fixing of bone edges has gone well, what should be marked in this image are the femur and tibia.
17. The program asks the user if the bone detection in this slice is correct. If it is, the program moves on to the next slice, but if it is not the user can manually fix the detection.
18. If the bone was not detected well automatically, the user can remove and add pixels to ensure there are no holes in the detected bone edges, which would cause (parts of) the bone to not be detected, and to ensure there are no areas outside the bone that are completely surrounded by edges, which would cause parts of the image that are not part of the tibia or femur to be incorrectly marked as bone.
19. Like before, the areas surrounded by edges are filled.
20. The femur and tibia as detected after manual correction as displayed.
21. The program asks if bone detection was correct, so if the manual correction was not successful, the user has the option to fix the edges further. This keeps going until the user is satisfied with the result and indicates that the bone segmentation has gone well.
22. The program moves on to the next slice.
23. Like in the previous slice, the script tries to automatically fix the detected edges and fill the holes surrounded by edges.
24. The automatically segmented femur and tibia are displayed.
25. If, after a number of slices, the slice that was displayed in the previous step no longer shows detectable bones, this meant the end of the joint has been reached and bone segmentation is no longer possible or necessary. This slice should therefore no longer be included in the segmentation and the user has to option to indicate this. If it is not the last slice, the user can proceed to indicate if the bone detection is correct or, if not, fix it manually.
26. If the previous slice was the last, the entire process of steps 11-25 is repeated for the anterior direction instead of the posterior direction.
27. The femur and tibia have been completely segmented, represented by a binary matrix with 1's for pixels where bone was detected and 0's for pixels where no bones were detected. This matrix is smoothed to better represent the bone surface, as was explained in the Methods section. Different smoothing options were compared and the best result, where small irregularities were removed but the global shape of the bone was not altered, was gained when smoothing with a box filter sized 3x3x3 pixels.
28. The 3D isosurface reconstructions of the femur and the tibia are made.
29. Now that the 3D reconstruction has been made and the data is represented with a list of vertex coordinates instead of a 3D matrix, it is possible for the data to have non-rounded numbers. Since millimeters are a more interpretable measure than numbers of pixels and slices, the vertex coordinates are converted from pixel/slice indices to millimeters, giving a realistic 3D representation and enabling measurements in millimeters.
30. Data 3D reconstruction data as well as the matrices with the segmented femur and tibia are saved, to be used to create different outputs.

A.2 Automatic Edge Fixing

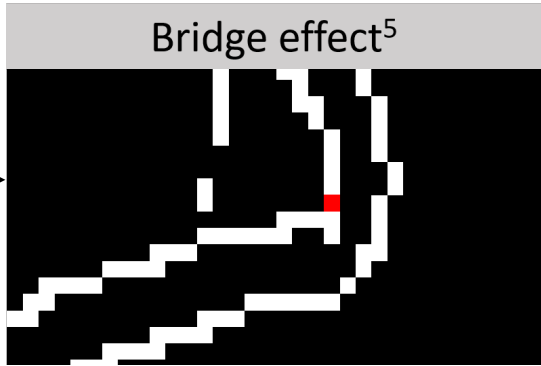
The automatic edge fixing, step 14 in the flow chart above, is explained more in detail in a separate flow chart below. Since this part of the process is fully automatic and more technical, not using the original image slice but binary images of detected edge pixel groups, just these binary images are used to explain different parts of the process. All steps are elaborated on in the pages after the flow chart.



Fill holes²

Number of pixels <80% of the previous slice?³

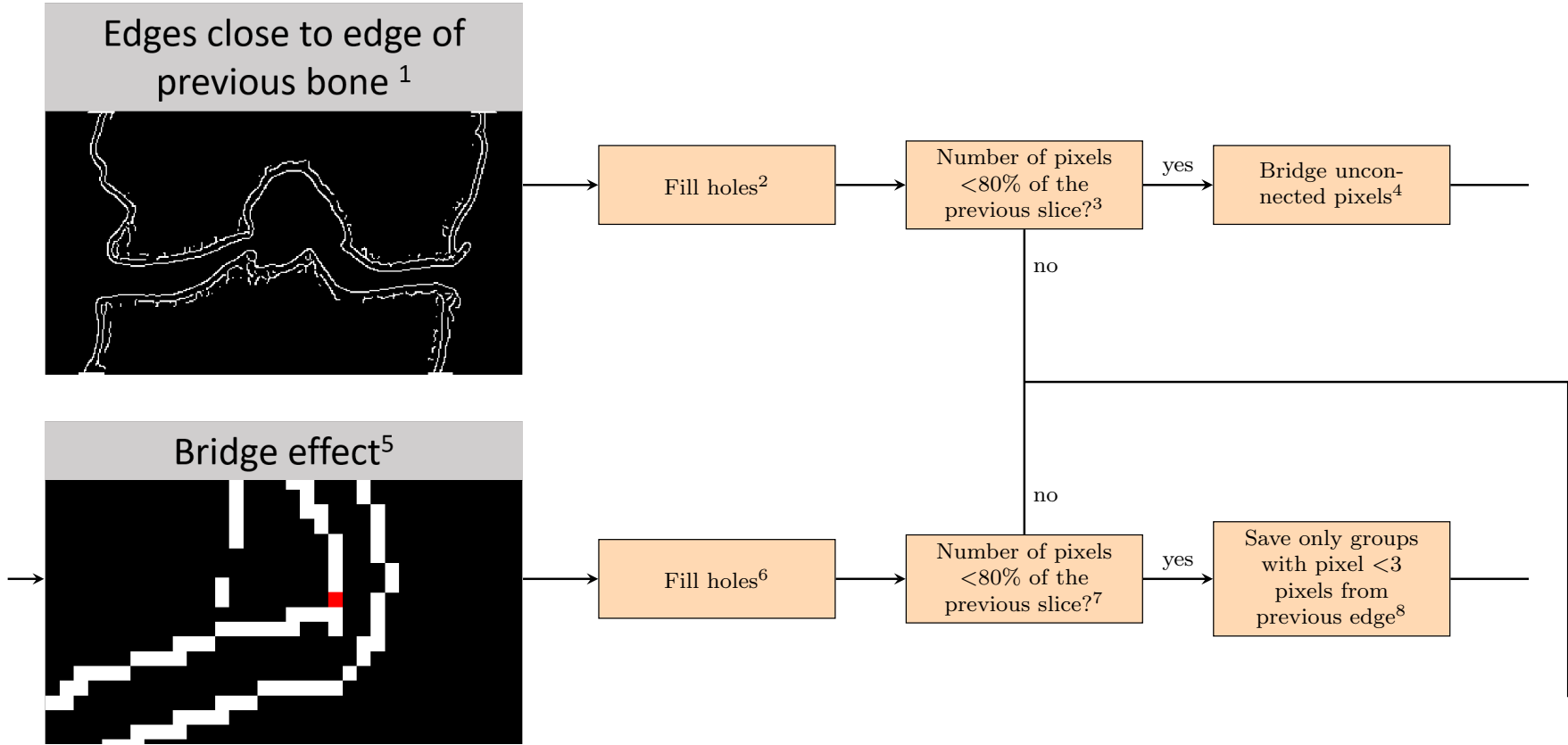
Bridge unconnected pixels⁴

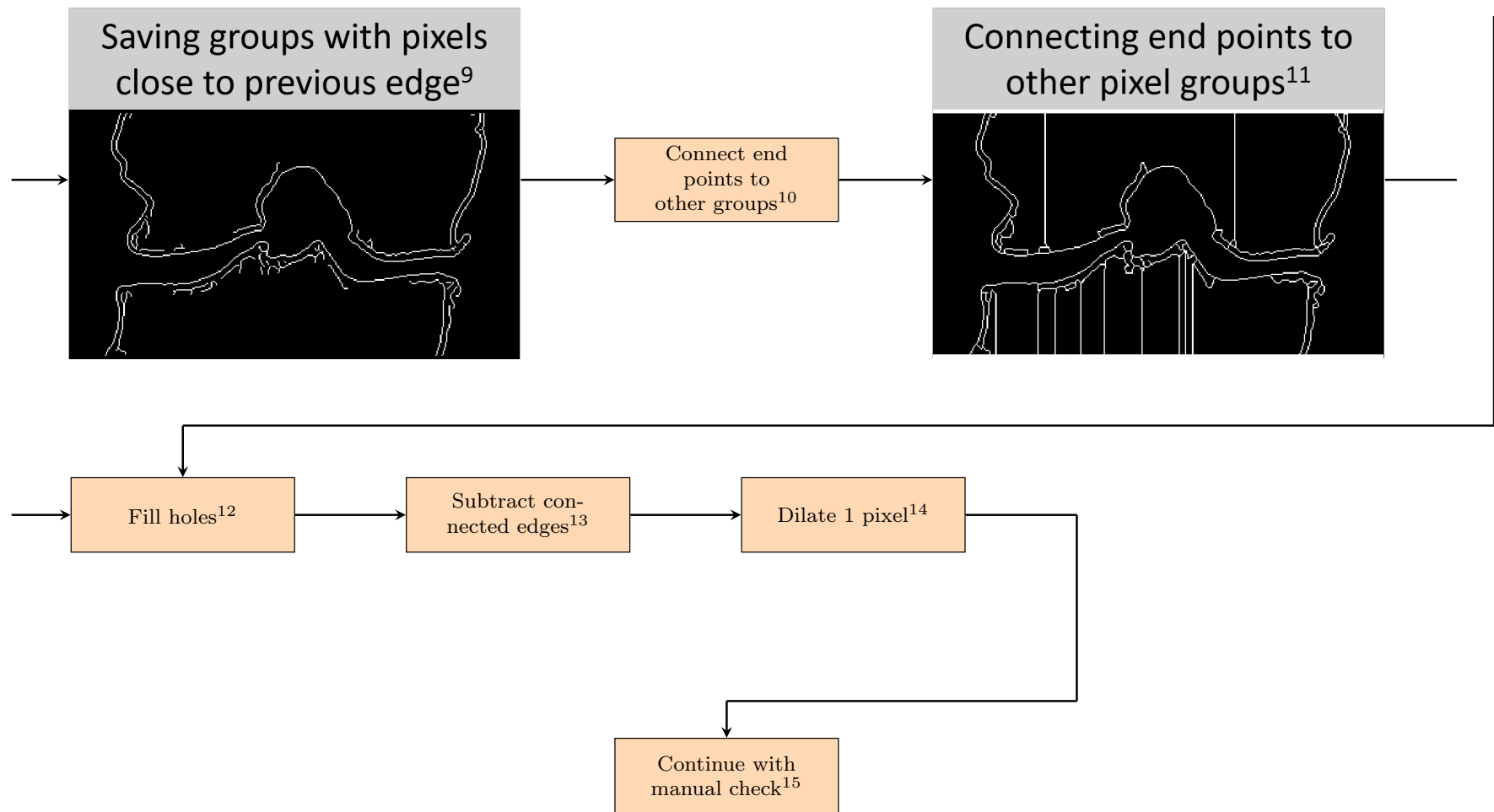


Fill holes⁶

Number of pixels <80% of the previous slice?⁷

Save only groups with pixel <3 pixels from previous edge⁸





1. As explained in step 12 of the previous flow chart, only pixels within 10 pixels distance from the outer lines of the bones segmented in the previous slice are saved. In this binary image, all edge pixels have value '1' and the rest has value '0'.
2. The holes in the edge image are filled, so all pixels in areas surrounded by edges are changed to '1'.
3. Since these are binary images, the number of pixels marked as bone (value = 1) can be counted by taking the sum of all pixel values. If this sum is less than 80% of the sum of bone pixels from the previous (already manually checked) slice, the bone marking must have gone wrong, since the slices are too thin for the bone to change so much between two slices. Therefore, the script tries to fix the detection.
4. The first try to fix the edges is to fill holes of one pixel by bridging pixels with value '0' that have two pixels of value '1' directly next to it.
5. Bridging is tried first since it cannot really alter the bone shape negatively. In this image, the pixel that would be added with bridging is shown in red.
6. The holes in the new (bridged) edge image are filled.
7. It is checked if, after bridging, the number of pixels marked as bone is still smaller than 80% of the previous slice. If it is, then more fixing is necessary.
8. Pixels groups are directly connected groups of pixels with value '1'. For example, in the image in step 5, bridging changed the number of pixel groups from five to four by connecting two different groups. Now, just the pixel groups that contain at least one pixel within three pixels of the bone edge of the previous slice are saved. This is some more filtering to save only the detected edges that could be bone, since the next step will only work well if there are (almost) no pixel groups outside the bone area.
9. The resulting edges after the filtering in the previous step. In this image it can be seen that filling the holes would not result in a filled femur and tibia. This can be seen best on the right top side of the tibia.
10. For every pixel group, the two end points are marked. All of these end points are then connected to another pixel group, closest to the end point. For example, for pixel groups A, B, C, D and E, the end points of pixel group A are connected to whichever group of B, C, D and E is closest to this end point. This connection is made the shortest way possible, so it does not matter where on the groups the end points connect to. All pixel groups are registered as separate groups before the connecting process begins, to ensure it is possible for two end points of one group to connect to the same group. For example, it is possible for both end points of group A to connect to group D if this is the closest for both, even if group A and D will be one group after the first end point connects.

Since, as explained for the previous flow chart, the edges are already separated in tibia edges and femur edges, depending on their position compared to the segmented bone from the previous slice, all groups are registered to either tibia and femur as well. Tibia pixel groups can only be connected to other tibia groups and femur groups can only be connected to femur groups.

Lastly, it is not desired that the connecting line from an end point crosses its own group, since this makes it likely extra parts outside the actual bone edge are added to the bone area. If this happens, the end point is not connected to the closest group, but instead connected to the top of the image in case of the femur and to the bottom of the image in case of the tibia. This way, the connecting line will almost always be inside the bone area.

11. The resulting edges after all group end points have been connected to other pixel groups. While there are many extra lines present that are no bone edges, these all fall in the bone area. Since eventually this entire area will be filled, so any edges present in the bone area are irrelevant. Filling this image will result in a segmented femur and tibia, since all holes in the edges around the bone area are now closed, even the right top part of the tibia.

12. All holes are filled again.
13. The edges as seen in step 11 are subtracted from the filled bone. This is done so that any separate edges outside the bone area are removed.
14. Subtracting the edges from the filled image removes the outer, one pixel thick layer of the bone, which is fixed by dilating the image one pixel.
15. Many holes in the edges are fixed by this automatic method, but it is not 100% perfect. Therefore, a manual check is still required. With this manual check, step 17 in the previous flow chart of the entire process is resumed.

A.3 Considerations

A number of things have been decided to be applied in the semi-automatic method that have not yet been explained:

- The effect of filtering perpendiculars by the angle between the tibia perpendicular and matching femur perpendicular. As explained shortly in the methods, the choice in this research has been to include only tibia perpendiculars for which the matching femur perpendicular (the perpendicular coming from the femur, originating closest to where the tibia perpendicular crosses the femur) also crosses the tibia. However, it is possible to filter more severely by allowing only a certain maximum angle between the pair of matching perpendiculars. The figure on the next page shows the effect of different maximum angles.

The top left figure shows all tibia perpendiculars crossing the femur, without checking if the corresponding femur perpendiculars cross the tibia surface. The top right figure shows only the tibia perpendiculars of which the matching femur perpendiculars cross the tibia surface. These are the perpendiculars that would be used in this thesis and it can be seen that many of the excessively large distances around the edge of the joint are removed, while the smaller distances remain. Furthermore, the perpendiculars are still rather evenly distributed throughout the plateau and the parts where the femur is expected to be are still included.

Limiting the perpendiculars to only those pairs that have an angle of 45 degrees or less (mid left figure) does not change the remaining pattern drastically, though a small area of perpendiculars disappears in the center of one of the tibial condyles, which is an area that is expected to be important in joint space measurements and cartilage degeneration. Making the angle limit even more severe by changing it to 30 (mid right figure), 25 (bottom left figure) or 20 (bottom right figure) degrees further reduces the number of perpendiculars in the centers of the tibial condyles.

Since matching three-dimensional perpendiculars between bones in the joint has not been described in literature, it was decided that more research is necessary before the optimal angle can be chosen and applied. Filtering out tibia perpendiculars of which the matching femur perpendicular does not cross the tibia plateau shows a clear improvement, even making the correlations with KIDA more significant, which is why this option was chosen as the used method in this research.

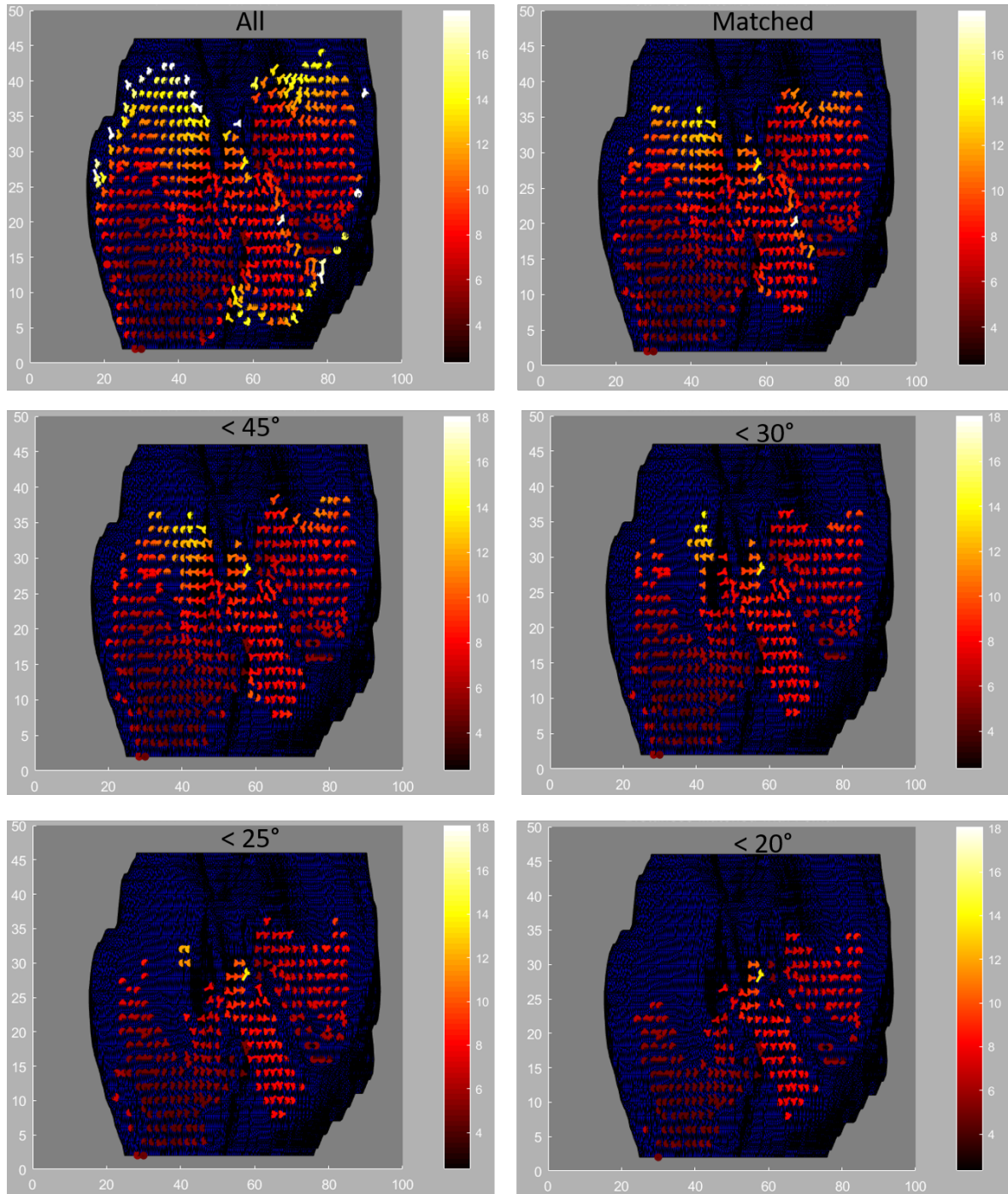


Figure A.1: The effects of matching tibia and femur perpendiculars compared to including all tibia perpendiculars crossing the femur (top left) either without angle limit (top right) or with four different angle limits (bottom four figures).

- Initially, when comparing the histograms and corresponding fitted lines of different scans, the areas under the curve (AUCs) were equalized. This can display the relative change in distances well, since results are scaled to the total amount of perpendiculars present. If, for example, the knee position of a patient would change between the baseline scan and the scan two years later, it is possible that this would cause a different amount of included perpendiculars. Equalizing the AUCs corrects for this. However, it was eventually decided to not equalize the AUCs. Looking at the tibia plateaus and perpendiculars at different time points for the same patient, there was no significant pattern difference seen. Furthermore, the amounts of smaller distances are not expected to change as much as a result of position change as the amounts of larger distances. Lastly, the absolute change in smaller differences between time points could be more relevant than the relative change, since this would directly indicate a change in small-distance area size.

Looking at the histograms for the MRI experiment, where knee positions were changed purposefully, the same conclusions are drawn from the equalized histograms as from the non-equalized histograms. Equalizing does clearly show different fits, but not enough research has been done as to what way the histograms should be shown to best represent the actual joint space changes. Therefore, it was decided to not edit the histogram representation, even for the MRI experiments. An important recommendation for now is to always look at the heat maps or perpendicular patterns as well as the histograms, so significant differences can be related to visual changes.

- When creating the difference heat map as seen in the results of the MRI experiment, the distances in one heat map are subtracted from the distances in the other heat map. More specifically, the different scans are first registered using the heat map shapes when using all tibia perpendiculars crossing the femur. These shapes are used, since they include most of the tibia plateau and are therefore easier to register. From this registration a registration matrix is made, which is then applied to the heat maps made from only tibia perpendiculars with matched femur perpendiculars crossing the tibia plateau. Lastly, the distances from one heat map are subtracted from distances from the other heat map at the exact same location.

On locations in the heat maps where only one of the maps has a distance and the other map is 'empty' (NaN), no resulting distance difference is saved. This way, only parts where both of the heat maps have distance values are included in the difference map and used for the SVD to calculate the change direction. However, if the location of matched perpendiculars on the tibia plateau changes (while the location of the non-matched perpendiculars does not), this indicates a shift in the tibia plateau that cannot be fully incorporated in the difference map and SVD calculation, since only the locations with matched perpendiculars overlapping between different scans will be included. Therefore, it could be better to also include parts where only one of the two heat maps has values. The reason this was not done in this research is that it is not straightforward how these parts should be included. For example, if after changing from an extended to flexed position causes perpendiculars to be located more posteriorly in the joint while perpendiculars more anteriorly disappear, this should cause the posterior change direction to be even greater than was already observed. So, locations where the second heat map contains distances but the first does not should cause a negative difference, but it is difficult to decide what this difference should be. It can be the opposite of the distance at that location, but that automatically means these distances become equally important to overlapping distances in calculating the SVD. Since not enough is known about what is important in these calculations and what is not, it was decided to alter the calculations as less as possible and therefore not include parts where only one of the two heat maps have values when calculating the difference map and SVD.

Technical details of performed scans

B.1 Radiographs

The exposure time and exposure varied between patients, the KVP and Source Image Distance were equal, as shown in the table below.

Manufacturer	Series	KVP (V)	Source image distance (mm)	Exposure time (range in ms)	Exposure (range in mAs)
Philips Medical Systems	Knee PA standing	66	1200	5-46	2-17

B.2 CT scans

For the patients' CT scans, many different scanners and scanning setting were used. The value ranges and the number of different possibilities as found in the data are listed in the table below.

	Manufacturer	Scanner model	KVP (V)	X-ray tube current (mA)	Exposure (mA)	Slice thickness (mm)	Pixel spacing (mm)
Options / range	Philips Medical Systems	Brilliance; iCT 256; Mx8000 IDT 16	100 - 140	69 - 323	75 - 150	1 - 2	0.276x0.276 - 0.793x0.793

B.3 MRI scans

The technical details of the MRI scans of patients used in this research as well as the scans performed in the MRI experiment are shown in the table on the next page.

Scan	Scanner	Protocol	Scanning Sequence	Sequence Variant	Slice thickness (mm)	Repetition time ms	Echo time ms	Magnetic field strength (T)	Acquisition Matrix	Flip angle (degrees)	Pixel spacing (mm)	Direction
Patient scans	Philips Medical Systems Achieva	3D Eckstein	Gradient Recalled (GR)	Spoiled (SP)	1.5	20	9.001	3	512 x 512	15	0.313 x 0.313	Coronal
MRI study	Esaote G-scan Brio	3D SHARC	Gradient Recalled (GR)	None	0.586	25	12.5	0.25	228 x 228	45	0.586 x 0.568	Coronal

MRI suitability form

ECTM

MRI screeninglijst

Screeninglijst voor een MRI-onderzoek

In de MRI ruimte kunnen sommige implantaten, apparaten en objecten beschadigd raken en/of schade aan u veroorzaken. Om gezondheidsrisico's zoveel mogelijk uit te sluiten moet iedereen voor toegang tot de MRI ruimte gescreend worden. Daarom verzoeken wij u onderstaande lijst zorgvuldig in te vullen.

Als u vragen heeft over de screening of een vraag met ja moet beantwoorden, kunt u elke werkdag contact opnemen met JK van Zandwijk; +31 (0)53 489 4197

Heeft u metaal(splinters) in uw lichaam, m.n. in de ogen, door bijv. werkzaamheden in de metaalindustrie (lassen, draaibankwerken etc.) of door oorlogsgeweld (geweerhagel, kogelresten, metaalscherven)?	<input type="checkbox"/> ja	<input type="checkbox"/> nee
Heeft u een pacemaker, pacemakerdraden of een defibrillator voor uw hart?	<input type="checkbox"/> ja	<input type="checkbox"/> nee
Heeft u een nieuwe hartklep/aortaklep of een stent?	<input type="checkbox"/> ja	<input type="checkbox"/> nee
Heeft u clips in de bloedvaten van het hoofd of overige bloedvaten?	<input type="checkbox"/> ja	<input type="checkbox"/> nee
Heeft u geïmplanteerde magneetjes in de kaak?	<input type="checkbox"/> ja	<input type="checkbox"/> nee
Heeft u gehoorbeenprothese / blaasstimulator / insulinepompje / neurostimulator / baclofenpomp / tissue expander?	<input type="checkbox"/> ja	<input type="checkbox"/> nee
Heeft u oor- oogimplantaten?	<input type="checkbox"/> ja	<input type="checkbox"/> nee
Zijn er lichaamsvreemde materialen in uw lichaam aanwezig / ingebracht?	<input type="checkbox"/> ja	<input type="checkbox"/> nee
Bent u zwanger?	<input type="checkbox"/> ja	<input type="checkbox"/> nee
Heeft u een beugel (of draad) van metaal die in de mond vast zit?	<input type="checkbox"/> ja	<input type="checkbox"/> nee
Heeft u piercings?	<input type="checkbox"/> ja	<input type="checkbox"/> nee

Op alle vragen nee?

Deze lijst ingevuld en ondertekend inleveren bij degene die u de lijst heeft toegereikt of toegezonden.

Let op:

Metalen, elektrische of magnetisch gevoelige voorwerpen kunnen niet de MRI ruimte in omdat er een sterke magneet aanwezig is in de ruimte. Denk hierbij aan; creditcards, pinpasjes, gehoorapparaten, mobiele telefoon, horloge, sleutels, haarspelden, sieraden, bril en munten.

Naam:

Handtekening:

Datum:

Technical Medicine Master of Science Thesis

Mylène Jansen, BSc

UNIVERSITY OF TWENTE.



UMC Utrecht